Water dynamics in NH_2-MIL-125: insights from a combined ^{1}H NMR relaxometry and computational investigation

Journal:	*The Journal of Physical Chemistry*
Manuscript ID	jp-2021-02045u.R2
Manuscript Type:	Article
Date Submitted by the Author:	n/a
Complete List of Authors:	Pizzanelli, Silvia; National Research Council (CNR), Istituto di Chimica dei Composti OrganoMetallici (ICCOM) freni, angelo; ICCOM CNR Pisa, Hajiahmadi Farmahini, Amir; The University of Manchester, Department of Chemical Engineering and Analytical Science Gordeeva, Larisa; Institut kataliza imeni GK Boreskova SO RAN; Novosibirsk State University Sarkisov, Lev; University of Edinburgh, Institute for Materials and Processes Solovyeva, Marina V.; Boreskov Inst Catalysis, Forte, Claudia; Consiglio Nazionale delle Ricerche, Istituto di Chimica dei Composti OrganoMetallici

Water Dynamics in NH_2-MIL-125: Insights from a Combined ^1H NMR Relaxometry and Computational Investigation

*Silvia Pizzanelli[†], *, Angelo Freni[†], Amir H. Farmahini[‡], Larisa G. Gordeeva[§, ♯], Lev Sarkisov[‡], Marina V. Solovyeva[§], and Claudia Forte[†]*

[†] Istituto di Chimica dei Composti OrganoMetallici (ICCOM), Consiglio Nazionale delle Ricerche – CNR, via G. Moruzzi 1, 56124 Pisa, Italy

[‡] Department of Chemical Engineering and Analytical Science, the University of Manchester, Manchester, M13 9PL, United Kingdom

[§] Boreskov Institute of Catalysis, Ac. Lavrentiev av. 5, Novosibirsk 630090, Russia

[♯] Novosibirsk State University, Pirogova str. 1, Novosibirsk 630090, Russia

Corresponding Author

* Silvia Pizzanelli, ICCOM-CNR, via G. Moruzzi 1, 56124 Pisa, Italy. Phone: +39 0503152549; E-mail: silvia.pizzanelli@pi.iccom.cnr.it

ABSTRACT

The dynamics of water confined in a microporous metal organic framework was investigated by ^{1}H Fast Field Cycling Nuclear Magnetic Resonance (NMR) relaxometry exploring time scales ranging between 10 μs to 0.1 ns in the 25-80 °C temperature interval. The data were interpreted within a dynamic model where molecules bind to the surface hopping among preferential binding sites. The bound molecules are also subject to local faster reorientations. Numerical analysis of the data allowed the characteristic times associated to hops and local anisotropic reorientations to be determined together with their activation energies, as derived through Arrhenius fits. The values of the activation energies, 16 ± 2 kJ/mol and 4.5 ± 0.5 kJ/mol, respectively, were rationalized within the model. ^{1}H Magic Angle Spinning NMR was used to quantify the water loading level and to obtain evidence on the presence of bound water molecules as required by the dynamic model, whereas molecular simulations were conducted to obtain complementary information on relevant properties, such as the porosity of the matrix, the water binding sites, self-diffusion and interaction energies in the confined space.

Introduction

Guest dynamics inside porous media affects the rates of many physical, chemical, and biochemical processes and is therefore important to both scientists and engineers in many contexts for both fundamental and practical reasons. Dynamics of guest molecules in porous solids can be quantified by a variety of microscopic techniques. Besides Pulse Field Gradient (PFG) Nuclear Magnetic Resonance (NMR), Fast Field Cycling (FFC) NMR has been widely employed to investigate fluids confined in porous materials exploring dynamic processes characterized by frequencies in the range 10 kHz-tens of MHz, corresponding to the Larmor frequencies at which spin lattice relaxation times are measured.[1] Adsorption and transport processes can be explored on a molecular level using molecular simulations, providing insight into translational and rotational motions of confined species on time scales of 10^{-3}-100 ns. Together with the computational structure characterization, these techniques form a powerful set of tools to complement the experimental measurements. [2]

In this study, we investigated the dynamics of water confined in the metal organic framework (MOF) NH_2-MIL-125 exploiting ^{1}H FFC NMR with the support of solid state NMR and molecular modeling. To the best of our knowledge, this is the first time FFC NMR is applied to a MOF with the aim of studying the dynamics of a guest molecule, although some of us have applied this technique to explore the dynamics of the amino group of the matrix and its electronic environment.[3] On the other hand, PFG NMR has been employed to study diffusivity of water or other small molecules in a few MOFs[4,5,6,7,8] and several investigations using molecular modeling have been reported regarding water in MOFs.[9,10,11,12,13,14,15,16]

Among the profusion of nanoporous materials available today, MOFs are outstanding for the variety of potential applications. NH_2-MIL-125, in particular, has been found to exhibit promising properties in the field of adsorption heat transformation and storage [17,18,19] due to its high adsorption capacity

(particularly for water), stability, low regeneration temperature, minor sensitivity of adsorption capacity and of porosity to adsorption cycles, and demonstrated efficiency in the adsorption chilling cycle with water as working fluid. The latter property is mainly governed by the sorption rate and depends, inter alia, on water dynamics. However, little is known on what influences water dynamics in MOF structures and, to the best of our knowledge, only one study has been published reporting the transport diffusion coefficient of water in this particular MOF. [20]

FFC NMR data of water in a completely filled MOF were collected in the temperature range 25-80 °C and interpreted within a model developed for the dynamics of liquids confined in porous solids, [21] where molecules bound to the surface hop among preferential binding sites. In addition, solid state ^{1}H NMR Magic Angle Spinning (MAS) was used to quantify the water loading level in the MOF and to obtain evidence of the presence of a fraction of bound water molecules, as required by the model. Molecular simulations were conducted to support and strengthen the picture delineated by the dynamic model, focusing on the pore structure, the water binding sites, the energy of water/water and water/MOF interactions and self-diffusion.

Materials and Methods

1. Preparation of the samples

NH_2-MIL-125 was synthesized according to the procedure by Gordeeva *et al*. [18] The as-synthesized product was constituted by primary particles, with an average size of about 1.8 μm.[22]

For the NMR measurements, the primary particles were dried *in vacuo* at 150 °C for 20 hours. The powder was then exposed to a humid atmosphere to progressively hydrate the sample. The hydration level, measured gravimetrically and double-checked using the ^{1}H NMR signal calibration, is reported

throughout the text in terms of pore-filling factor, θ. Samples characterized by θ=0.09, 0.22, 0.55, and 1.00 were prepared. The maximum amount adsorbable was 0.45 g per g of dry powder.[22]

2. NMR measurements

2.1 Solid state NMR. Solid state ^{1}H and ^{13}C NMR experiments were performed on a Bruker Avance Neo-300 WB spectrometer equipped with a 4 mm probe. The operating frequencies were 300.13 and 75.47 MHz for ^{1}H and ^{13}C, respectively. The ^{1}H MAS spectra were recorded using a single 90° excitation pulse of 4.5 μs and accumulating 64 transients with a repetition delay of 1 s and a spinning speed of 10 kHz. The experiments were performed at 25, 40 and 80 °C; temperature was controlled by a BVT 1000 (Eurotherm) variable-temperature unit, with a temperature stability of ± 0.1 °C. The ^{13}C direct excitation spectrum of the MOF at the filling factor 0.09 was recorded using a 90° excitation pulse of 4.5 μs and accumulating 750 transients with a recycle delay of 120 s. The $^{13}C/^{1}H$ correlation spectrum of the same sample was acquired using frequency-switched Lee-Goldburg (FS-LG) irradiation during the evolution with a CP contact time of 6 ms, a ^{1}H 90° pulse and a magic-angle pulse lengths of 3 μs and 1.8 μs, respectively, a duration of successive FS-LG pulses of 9.8 μs and accumulating 128 transients, using a rotor spinning speed of 12 kHz.

2.2 FFC NMR relaxometry. The ^{1}H longitudinal relaxation times (T_1) values were measured in the 0.01 - 35 MHz Larmor frequency range using a SpinMaster FFC-2000 Fast Field-Cycling NMR relaxometer (Stelar srl, Mede, Italy). The experiments were performed using the pre-polarized and non-polarized pulse sequences below and above 12 MHz, respectively. The polarizing and detection fields were 0.60 T and 0.50 T, corresponding to ^{1}H Larmor frequencies of 25.0 and 21.5 MHz, respectively. The switching time was 3 ms and the 90° pulse duration 9.8 μs. The dead time was 14.5 μs. A single scan was acquired. All the other experimental parameters were optimized for each measurement. All the ^{1}H magnetization curves *vs* time were monoexponential within experimental error and the errors in the

relaxation rates R_1 (=1/T_1) obtained from the fitting of the curves were always lower than 1 %. The monoexponentiality is evidence for the absence of water between the powder grains in the completely filled sample. Measurements were performed in the temperature range 25-80 °C. The temperature was controlled within ± 0.1 °C with a Stelar VTC90 variable temperature controller.

2.3 Theoretical basis and data analysis. The spin lattice relaxation rate, arising from the modulation of the intramolecular dipolar interaction between the two protons in a water molecule caused by suitable molecular motional processes, is given by the following equation[23]

$$R_1 = \frac{1}{T_1} = K[J(\nu) + 4J(2\nu)] \quad (1)$$

where $K = \left(\frac{3}{20}\right)\left(\frac{\mu_0}{4\pi}\right)^2 \gamma^4 \frac{\hbar^2}{a^6}$, with μ_0 the vacuum permeability, $\hbar$ the reduced Planck constant, γ the proton gyromagnetic ratio, and a the interproton distance. For the water molecule, K was fixed to $8 \cdot 10^9$ s^{-2},[24] corresponding to a=1.5 Å. The spectral density $J(\nu)$ is related to the water molecule dynamics. In the porous space, two different situations can be envisaged for the water molecules:

1) free water molecules which do not interact with the surface and can be safely assumed to be subject to fast isotropic molecular reorientations and self-diffusion
2) water molecules bound to the surface experiencing fast anisotropic molecular reorientations that do not average out the intramolecular dipolar proton interaction which is further modulated by slower dynamic processes occurring on the time scales probed by FFC NMR relaxometry.

For the water molecules close to the pore surface, a slower process could be identified with the hopping of the molecules among preferential binding sites on the surface with reorientation being a consequence of the displacements along the surface. This motion can be described according to the so-called Reorientations Mediated by Translational Displacements (RMTD) model.[21]

However, it must be noted that the water molecules can exchange between different states. Since monoexponential relaxation was observed, the exchange between the bound and free state and between different bound states is certainly *fast with respect to the spin lattice relaxation rate*. Proton exchange between water and OH and NH_2 groups in the matrix, as well as proton transport are also expected to occur but on much longer time scales than those accessible to the FFC NMR technique,[1] with the result that these processes will not give rise to any dispersion in the FFC data in the available frequency window.

If the local molecular reorientations are much faster than the exchange of molecules between the two water pools and if the *exchange is slower than the RMTD process*, the spectral density $J(\nu)$ can be expressed as a linear combination of contributions from the different dynamic processes, that is, $J_{LR}(\nu)$ due to both isotropic and restricted local molecular reorientations and $J_{RMTD}(\nu)$ due to the RMTD mechanism:[25]

$$J(\nu) = J_{LR}(\nu) + J_{RMTD}(\nu) \quad (2)$$

Indeed, in strongly adsorbing matrices water exchange between the two pools has characteristic times longer than 10^{-5} s.[1,21,26,27] Therefore, within the proposed scenario, molecular orientation relative to the surface is more or less reestablished after each hopping event and many hopping events occur during the exchange time before correlation to the initial orientation is finally lost. Moreover, the molecules remain bound to the surface for a time exceeding the correlation time associated to the anisotropic reorientation.

The spectral densities for the rotational motions can be expressed according to Bloembergen-Purcell-Pound (BPP) equation:[25,28]

$$J_{LR}(\nu) = p_b(1 - S^2)\frac{2\tau_{RR}}{1 + (2\pi\nu\tau_{RR})^2} + (1 - p_b)\frac{2\tau_{IR}}{1 + (2\pi\nu\tau_{IR})^2} \quad (3)$$

while the spectral density for the RMTD process can be described by the following equation:[25]

$$J_{RMTD}(\nu) = \frac{A_{RMTD}}{(2\pi\nu)^{1/2}}\left[f\left(\frac{\nu_{RMTD,max}}{\nu}\right) - f\left(\frac{\nu_{RMTD,min}}{\nu}\right)\right] \quad (4)$$

with $f(x) = \arctan\left(\sqrt{2x}+1\right) + \arctan\left(\sqrt{2x}-1\right) - \operatorname{arctanh}\left(\frac{\sqrt{2x}}{x+1}\right)$. The relevant parameters are: (i) the fraction of bound molecules, p_b; (ii) the order parameter representing the residual correlation of restricted tumbling, S; (iii) the correlation times for restricted, τ_{RR}, and isotropic, τ_{IR}, local reorientations, associated to bound and free water, respectively; (iv) the parameters A_{RMTD}, $\nu_{RMTD,max}$ and $\nu_{RMTD,min}$ related to the RMTD model. For this model, we assumed that the hops among binding sites are described as a two-dimensional normal diffusion process and that a distribution of RMTD correlation times, and hence of RMTD characteristic frequencies, ν_{RMTD}, occurs. As an ansatz, equally-weighted characteristic frequencies were assumed between a minimum and maximum cut-off frequency, $\nu_{RMTD,min}$ and $\nu_{RMTD,max}$, respectively, considering that a purely stochastic distribution of orientations might describe the rugged surface topology of the MOF. The cut-off frequencies are defined as

$$\nu_{RMTD,max} = \frac{q_{max}^2 D}{2\pi} \quad (5)$$

$$\nu_{RMTD,min} = \frac{q_{min}^2 D}{2\pi} \quad (6)$$

where q_i identifies a diffusion mode and is related to the surface structure, and D represents the diffusion coefficient on the surface.

A_{RMTD} is given by the following expression

$$A_{RMTD} = \frac{\sqrt{2} p_b S^2}{\Delta q D^{1/2}} \quad (7)$$

with $\Delta q = q_{max} - q_{min}$, where q_{max} and q_{min} are as defined above.

The minimum and maximum cut-off frequencies, $\nu_{RMTD,min}$ and $\nu_{RMTD,max}$, can be related to the minimum and maximum distances beyond which the reorientational correlation begins to decay, l_{min} and l_{max}, respectively, through the following equations:

$$l_{min} = \sqrt{\frac{4D}{2\pi\nu_{RMTD,max}}} \quad (8)$$

$$l_{max} = \sqrt{\frac{4D}{2\pi\nu_{RMTD,min}}} \quad (9)$$

Self-diffusion can also contribute to relaxation but its contribution is negligible. In fact, applying the Torrey model,[29,30] with the density set equal to that of bulk water, the self-diffusion coefficient to the value of 1.23 10^{-10} m^2/s found with MD simulations at 25 °C (see paragraph *Water self-diffusivity and interaction energies from molecular simulations* in the Results and Discussion section), and the average jump distance and the distance of closest approach to values between 3 and 5 Å, the contribution of the self-diffusion mechanism to relaxation is only about 1 s^{-1} in the whole frequency range examined.

The analysis of the ^{1}H FFC NMR data in terms of the model described was performed using the least-squares minimization procedure implemented in the Fitteia environment.[31,32]

3. Molecular simulation methods

3.1 Structural and binding sites analysis. The cif-file for NH_2-MIL-125 has been previously used in the study by Vaesen *et al.*[33] on adsorption of gases in this material. Structural analysis was performed using the Poreblazer v4.0 software for computational characterization of porous materials based on the lattice representation of the porous space.[34] The methods employed in the software, along with the tutorial

case studies, are provided online and have been recently reviewed by Sarkisov *et al*. in application to the CSD MOF database.[34] In the case of NH_2-MIL-125, Poreblazer was predominantly used to obtain values of the accessible surface area, occupiable pore volume, pore limiting diameter, and pore size distribution (PSD). In addition, we used Poreblazer to visualize the structural organization of porous space within NH_2-MIL-125. The parameters associated with these calculations and other properties given by Poreblazer are reported in the SI. To characterize the binding sites and the free energy landscape within the porous space of NH_2-MIL-125, we employed the methods described by Sarkisov.[34,35] Briefly, similarly to the Poreblazer approach, the porous space of the material under investigation was discretized into a fine lattice (0.2 Å), the probe molecule was then placed into the centre of the lattice site and its interaction with the porous materials was probed for different orientations of the molecule. This allows the Helmholtz free energy in the specific site location to be estimated, while the percolation analysis based on the Hoshen-Kopelman algorithm allows the free energy barriers and favorable interaction energy sites in zero loading regime to be characterized. For the complete details of the methodology we refer the reader to the original publications,[34,35] while the specific parameters of the simulation in this study are provided in the SI.

3.2 Grand-canonical Monte Carlo simulation. Equilibrium adsorption isotherm of water vapour in the amino-functionalized NH_2-MIL-125 porous solid was modelled using the grand canonical Monte Carlo (GCMC) simulation method. In this study, GCMC simulations were performed using the RASPA 2.0 simulation package.[36] These simulations were used to validate the force field parameters employed in the study and to provide initial configurations of the adsorbed molecules for molecular dynamics simulation of diffusion properties. The adsorption isotherm was modelled at 25 °C and at 8 different pressure points below the saturation pressure of the employed water model. Simulations were run for approximately 780,000 cycles on average at each pressure point where every cycle consisted of N_{mc}

Monte Carlo trial moves. In RASPA, N_{mc} is equal to the average number of particles adsorbed in the system at a given pressure. The number of cycles for both equilibration and production stages of the simulations were kept equal. Within the simulation protocol, five different trial MC moves were attempted, specifically insertion, deletion, rotation, long-range and short-range translations. The atomistic structure of NH_2-MIL-125 was treated as a rigid framework consisting of 2 × 2 × 2 unit cells in periodic boundary conditions in three dimensions (with the original unit cell having dimensions of a = 18.673 Å, b = 18.673 Å, c = 18.138 Å). The 12–6 Lennard-Jones (LJ) potential model was employed to calculate dispersion (van der Waals) interactions, while long-range electrostatic interactions were treated using the Ewald summation. The potential cut-off distance for the dispersion interaction was set at 12 Å, while, for electrostatic interactions in real space, the cut-off was equal to 18 Å. Ewald precision variable was set to 10^{-6} in RASPA. Both LJ and electrostatic interactions were computed directly without the use of any grid potential. LJ parameters of the framework atoms, as well as their partial charges, were taken from a force field proposed by Vaesen *et al*.[33] For water, the TIP4P/2005 model developed by Abascal and Vega was employed.[37] In all GCMC simulations, pressure values were consistently converted to fugacity using the Peng–Robinson equation of state. The maximum amount adsorbed from the GCMC simulation on the ideal, defect-free model of a crystal is *ca.* 0.6 g/g at 25 °C.

In addition to equilibrium water uptake, we also calculated the enthalpy of adsorption at each pressure point using the energy-particle fluctuations in the grand-canonical ensemble (*i. e.* constant μVT) given by[38]

$$\Delta H_{ads} = \frac{\langle NU\rangle_\mu - \langle N\rangle_\mu \langle U\rangle_\mu}{\langle N^2\rangle_\mu - \langle N\rangle_\mu^2} - RT \qquad (10)$$

where $\langle\ldots\rangle_\mu$ refers to averages in grand-canonical ensemble, while N, U, R and T are the total number of adsorbed particles in the framework, the total potential energy of the system, the gas constant and

temperature, respectively. The equilibrium adsorption isotherm of water vapor and the loading-dependent enthalpies of adsorption for the same isotherm are provided in Figure S1, whereas the variation of water-water and water-MOF van der Waals and electrostatic interactions as a function of pressure are shown in Figures S2 and S3.

3.3 Molecular dynamics. We employed equilibrium molecular dynamics (EMD) to simulate self-diffusion of water in the porous structure of NH_2-MIL-125. The simulations were performed at 25 °C and at four different loadings using the LAMMPS simulation package.[39] The simulations were carried out in the canonical (*NVT*) ensemble in which the translational and rotational degrees of freedom of rigid adsorbate molecules were thermostated using the Nose–Hoover algorithm as described by Hoover[40] and Martyna *et al*. [41,42] To maintain the structure of rigid molecules for water, the flexibility of atomic bonds (bond length and bond angles) was constrained using the SHAKE algorithm. The atomistic structure of NH_2-MIL-125 was treated as a rigid framework consisting of a 2 × 2 × 2 cubic lattice with periodic boundaries in all three dimensions as in the GCMC simulations. A Verlet time integrator was used with time step equal to 1.0 fs. Short-range intermolecular interactions were modelled using the 12–6 Lennard–Jones potential with a cut-off distance of 12 Å. Long-range electrostatic interactions were modelled using the particle-particle particle-mesh (P3M) method[43] where the cut-off distance in real space and relative accuracy parameter of the model were set to 8.5 Å and 10^{-6}, respectively. MD simulations were performed at four different loadings corresponding to low (0.03 g/g and 0.05 g/g) and high (0.4 g/g and 0.6 g/g) loadings of water in the system. In terms of the pore-filling factor, θ, *i. e.,* the amount of water adsorbed divided by the maximum adsorbable amount, these loadings correspond to 0.005, 0.083, 0.67 and 1, respectively. Simulations were run between 46 to 145 ns after being fully equilibrated and were terminated after making sure that all water molecules had fully traversed the system.

To calculate self-diffusivity of water in NH_2-MIL-125, the mean-squared displacements (MSD) of the centres of mass of water molecules were collected in the Fickian regime in which the log–log dependence of the MSD with time has a slope equal to unity. Self-diffusion coefficients (D_{self}) were then estimated using the Einstein equation given by

$$D_{self} = \frac{1}{2Nd}\lim_{t\to\infty}\frac{1}{t}\left\langle \sum_{i=1}^{N} |r_i(t) - r_i(0)|^2 \right\rangle \quad (11)$$

where $r_i(t)$ is the vector associated with the centre of mass of molecule i at time t, N is the number of molecules, and d is the dimensionality of the system. It should be pointed out that D_{self} is different from the D parameter of the RMTD model (Eqs. 5-9); in fact, the former is related to water diffusing within the three-dimensional porous space, whereas the latter refers to water diffusing on the porous surface.

Results and Discussion

Structural characteristics of NH_2-MIL-125 and water loading analysis. The porosity of NH_2-MIL-125 was explored using the Poreblazer structural analysis. As can be seen from Figure 1, there are two types of pores, large pores of 10.65 Å and small pores of about 4-5 Å in diameter. In the x and y directions, these two types of pores are connected by short channels characterized by a pore limiting diameter of 3.77 Å, whereas, in the z direction, the system can be viewed as a chain of large pores of 10.65 Å size connected by channels with a 2.89 Å pore limiting diameter. Table 1 summarizes some relevant properties concerning NH_2-MIL-125 porosity published in ref. 18, from which the procedure for synthesizing the MOF was borrowed, together with the corresponding values calculated using the Poreblazer code. Other properties, obtained from Poreblzer, are summarized in the SI.

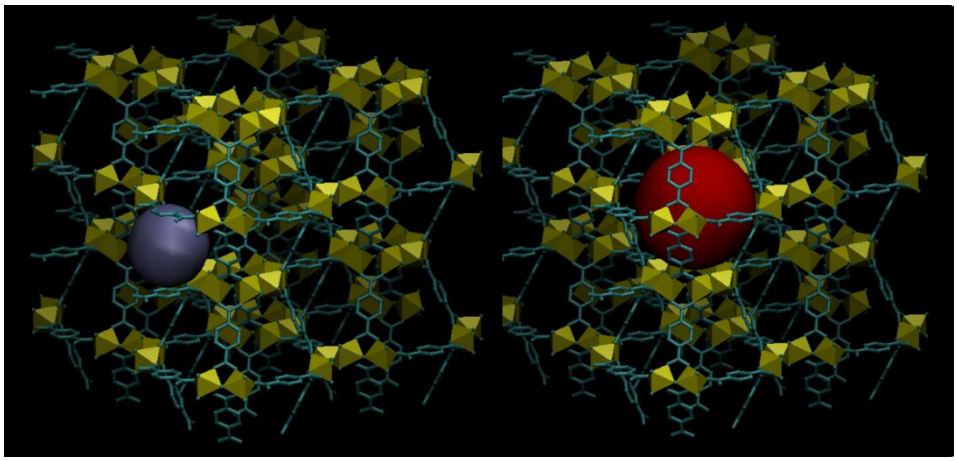

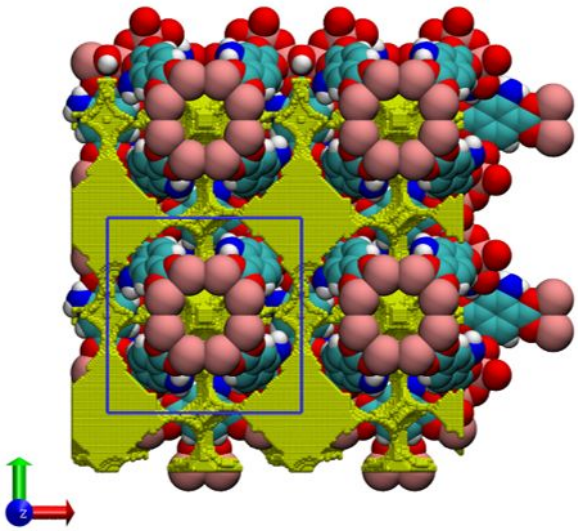

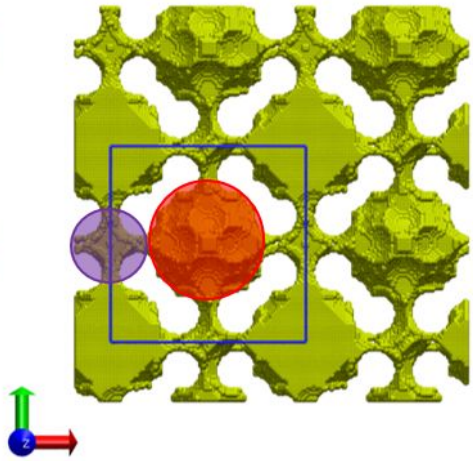

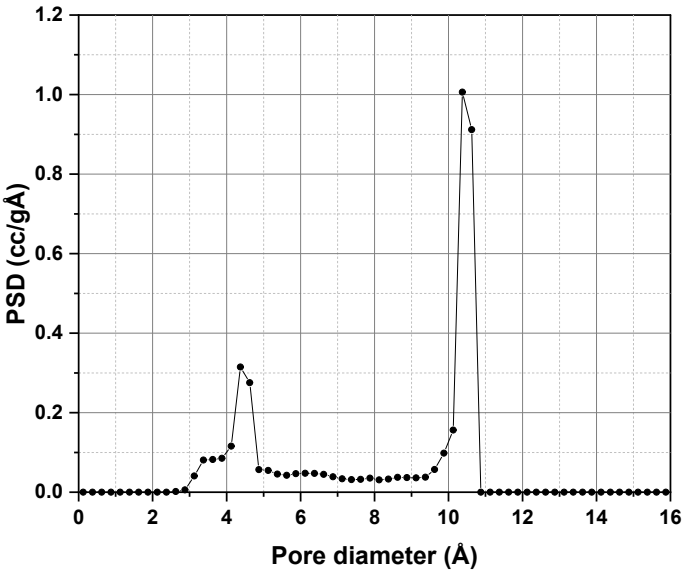
PSD (cc/gÅ)
Pore diameter (Å)
0.0
0.2
0.4
0.6
0.8
1.0
1.2
0
2
4
6
8
10
12
14
16

Figure 1. Structural characterization of NH_2-MIL-125. Top panel: the NH_2-MIL-125 is shown as cyan bond framework and yellow tetrahedra Ti-O units. The two main pores in the system are shown as encapsulated red (10.65 Å) and purple (4.5 Å) spheres. Middle panel: the structural organization of the pore network in NH_2-MIL-125 is shown as lattice of available sites (yellow). The network consists of intercalating small and large pores, connected by narrow windows. The pores identified in the top panel, are shown in this figure as red and purple circles. A single unit cell of NH_2-MIL-125 is indicated by the blue square. Other colors used are as follows: oxygen – red; carbon – cyan; titanium – pink; nitrogen – blue; hydrogen – white. Bottom panel: Pore size distribution from the Poreblazer code.

Table 1. Specific surface area, S, total pore volume, V_p, micro-pore volume, V_μ, of NH_2-MIL-125 primary particles.

S (m^2/g)	V_p (cm^3/g)	V_μ(cm^3/g)	Maximum amount of water adsorbed (g/g)	Ref.
1300[a]	0.56[a]	0.55[a]	0.45[a]	18
1389[b]		0.65[b]	0.60[c]	This work

[a] Values from nitrogen adsorption characterization.

[b] Values calculated using the Poreblazer code.

[c] Value calculated with GCMC.

As can be noted from Table 1, the surface area obtained from the computational structure analysis is in good agreement with the BET area obtained from nitrogen adsorption (ref. 18). The pore volume observed in the experiments is, however, much lower and this is possibly associated with partial structure collapse (which should also have an impact on the observed surface area) and the presence of residual solvent molecules.

The water loading level of the hydrated samples was checked by ^{1}H MAS NMR; the central band of the spectra at the four different hydration levels investigated is shown in Figure 2. Three main signals, resonating at 3.1, 4.5 and 7.9 ppm, were observed. The 4.5 and 7.9 ppm peaks were assigned to hydrogen atoms in water and in the aromatic rings of the linkers ($H_{aromatic}$), respectively. The 3.1 ppm peak was attributed to the methyl protons in residual methanol (H_{CH3}). This assignment was supported by $^{13}C/^{1}H$ correlation spectrum (Figure S6). Analysis of the ^{13}C direct excitation NMR spectrum (Figure S5) indicated that the residual methanol amounts to 1 molecule per BDC unit. It is noticeable that, even after activation at 150 °C *in vacuo* for 20 hours, residual methanol is present; this, however, can be explained considering that methanol is used in the synthesis of the MOF and, given the small channel dimensions compared to the kinetic diameter of the methanol molecule (3.8-4.1 Å),[44] it may remain trapped in the pores during MOF formation. Indeed, this points to a plausible contribution to the difference in the experimental pore volume and pore volume of an ideal crystal, presented in Table 1.

The water amount was determined through the deconvolution of the ^{1}H spectra, as exemplified in Figure 2b for the sample characterized by θ=0.55. The deconvolution allowed the relative intensities of the signals to be determined from which the relative amounts could be evaluated. The intensity of the ^{1}H signal resonating at 4.5 ppm was proportional to the hydration level expressed in grams of water per grams of dry MOF. This proportionality, within the experimental error, is shown in Figure 3, where the peak intensity is scaled imposing that the residual methanol signal intensity is equal to 3, the number of methyl protons for each BDC unit, in agreement with the finding that there is one methanol molecule per BDC unit. The line in the figure represents the linear fitting curve, characterized by an intercept of 3.0 ± 0.7. This agrees with the value expected on the basis of stoichiometry, *i. e.* 3.67, calculated as the sum of amine and hydroxyl hydrogen atoms which are assumed in fast exchange with water protons in the hydrated samples. For each residual methanol molecule, there are 2 amine hydrogen atoms carried by a BDC unit, 0.67 hydroxyl hydrogen atoms from Ti-OH-Ti, and 1 hydroxyl hydrogen atom from the

methanol. These protons were not detected in the spectra, confirming that amine and hydroxyl protons were in fast exchange with water protons, with exchange times shorter than about 10^{-3} s, i. e. the inverse of the frequency difference between the signals of the not exchanging species.[45,46] The exchange of the amine and Ti-OH-Ti hydroxyl protons with water was also demonstrated by means of IR spectroscopy on samples exposed to D_2O vapor.[33]

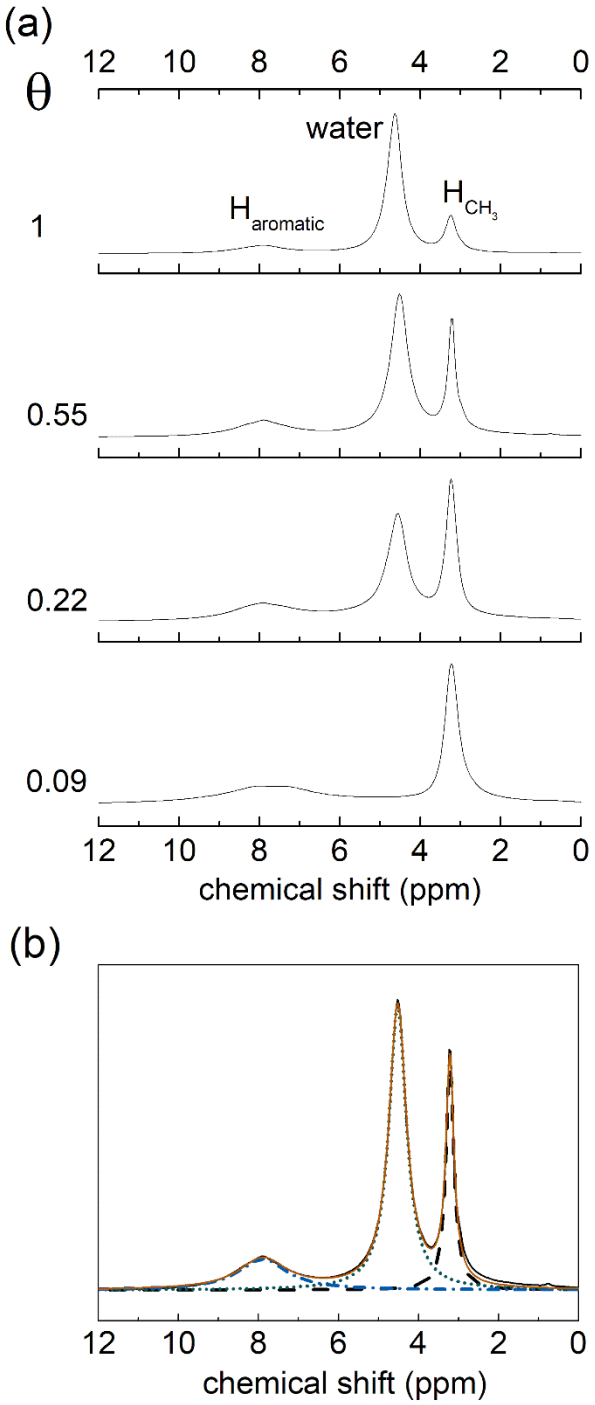

Figure 2. (a) Central band of ^{1}H MAS spectra of NH_2-MIL-125 at different hydration levels expressed through the pore-filling factor θ. The three main signals are assigned to hydrogen atoms of water, of the linker aromatic ring ($H_{aromatic}$), and of methyl groups in residual methanol (H_{CH3}). (b) Spectrum at θ=0.55, showing the Lorentzian peaks obtained from a deconvolution; the green short dotted peak

centered at 4.5 ppm is due to water, the blue short dash dotted peak centered at 7.9 ppm is due to $H_{aromatic}$, and the black dashed peak centered at 3.1 ppm is due to H_{CH3}. The sum of the peaks is displayed as a red solid line.

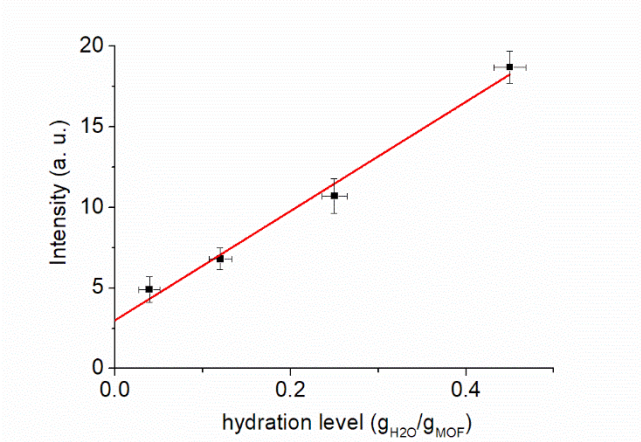

Figure 3. Intensity of the ^1H signal resonating at 4.5 ppm as a function of the hydration level expressed in grams of water per grams of dry MOF. The intensity of this peak is scaled imposing that the residual methanol signal intensity is equal to 3, the number of methyl protons for each BDC unit. The line represents the linear fitting curve, characterized by an intercept of 3.0±0.7.

The number of water molecules per BDC unit in the sample characterized by θ=1 is about 7. This value is obtained from the intensity of the signal resonating at 4.5 ppm (equal to 18 in the scale employed in Figure 3), after subtraction of the contribution to the signal from exchangeable protons (equal to 3 on the same scale, as indicated by the intercept value in Figure 3) and divided by 2 for the two protons in each water molecule. Since every 6 BDC units there is one large cage, two small cages, and windows connecting them, we estimate that about 40 water molecules occupy this porous space. According to Poreblazer estimates, the volume of the largest cage is about 700 $Å^3$ and, if we assume bulk water density (*i. e.*, 1 g/cm^3), such pore should contain about 25 water molecules. The smaller cage is about

30 Å^3 and can contain maximum 2-3 water molecules, so that the predicted number of water molecules occupying cages in a completely filled MOF is about 30. This picture is also confirmed using molecular dynamics and population analysis of the cages (see the SI, Figure S4). We hypothesized that the water molecules in the sample characterized by θ=1 are located both in the cages and in the windows connecting them.

Presence of bound water molecules. ^{1}H MAS was also used to obtain evidence supporting the presence of two types of water molecules. Figure 4 shows ^{1}H MAS spectra of the completely filled sample at three selected temperatures, 25, 40 and 80 °C. It can be observed that the central band is flanked by first order side bands of low intensity relative to the water signal and to the signal due to the aromatic hydrogen atoms of the BDC linkers. The side band relative to the signal occurring at 3.1 ppm (that is, the signal at about 36.5 ppm in the upper trace of Figure 4) has a structured line shape, which is particularly evident in the spectrum recorded at 80 °C. This is due to a small fraction of N-H hydrogen atoms not exchanging with water and resonating in the same region as the methyl protons of methanol. Similar line shapes are predicted for protons bonded to amino nitrogen nuclei considering the ^{14}N quadrupole effects on the ^{14}N-^{1}H dipolar interaction.[47] The occurrence of a distinct signal for this type of protons indicates that these protons do not exchange with water possibly because these particular amino groups are located in regions not accessible to water. In addition, simple inspection of the water signal, at about 4.5 ppm, revealed that it shifted upfield and sharpened upon heating, and the intensity of its side bands tended to decrease. The shift was attributed to a variation of the hydrogen bond network with temperature. The presence of side bands, although weak and decreasing with increasing temperature, indicated that, for a fraction of water molecules, the dipolar interaction between the two hydrogen atoms was not completely averaged out by MAS. This fraction was identified with water molecules bound to the surface.

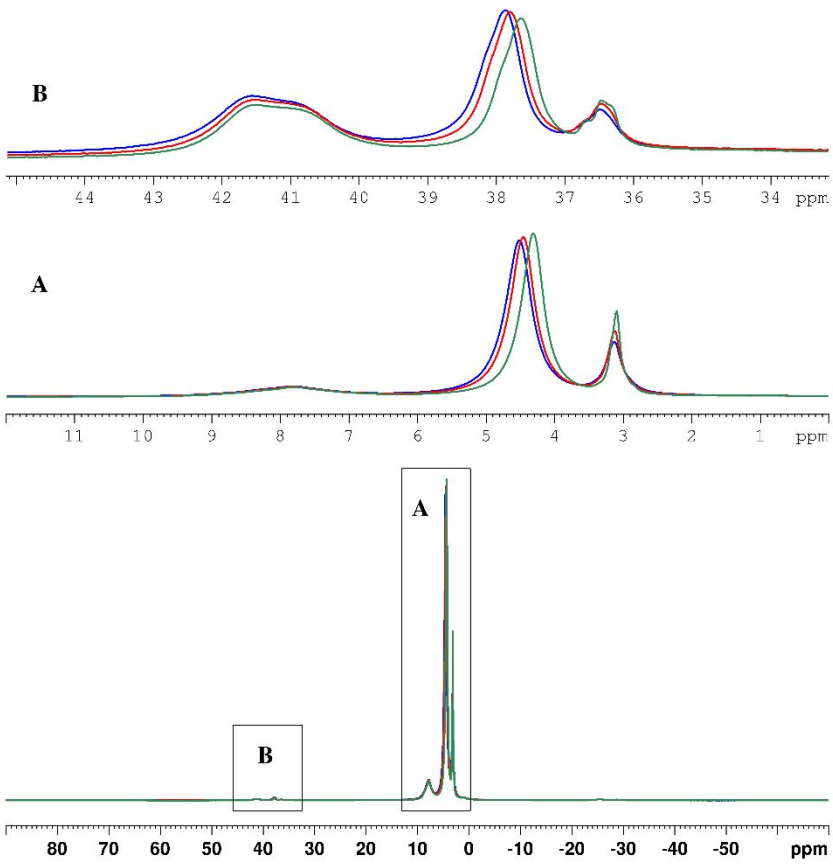

Figure 4. ^{1}H MAS spectra of NH_2-MIL-125 at θ=1 at 25 (blue line), 40 (red line) and 80 (green line) °C (lower trace) and expansion of the central band labeled A (middle trace) and of the first order side band on the left side labeled B (upper trace). The vertical scale in the upper trace is decreased by a factor of 95 compared to that of the lower trace.

Water preferential binding sites and free energy barriers from molecular simulations. The affinity of water molecules towards potentially hydrophilic atomic sites in the porous structure of NH_2-MIL-125 was explored using radial distribution functions (RDF) from MD simulations and analysis of the binding sites using lattice methods as described in the Methodology section. RDF was calculated for three different atomic pairs: (1) water oxygen and BDC nitrogen, (2) water oxygen and MOF titanium, and (3) water oxygen and hydroxyl oxygen in MOF. Nitrogen, titanium and hydroxyl oxygen atoms

possess large partial charges which make them interesting candidates for binding water based on the importance of electrostatic interactions (see Figure S3). The RDFs calculated for the three atomic pairs are illustrated in Figure 5.

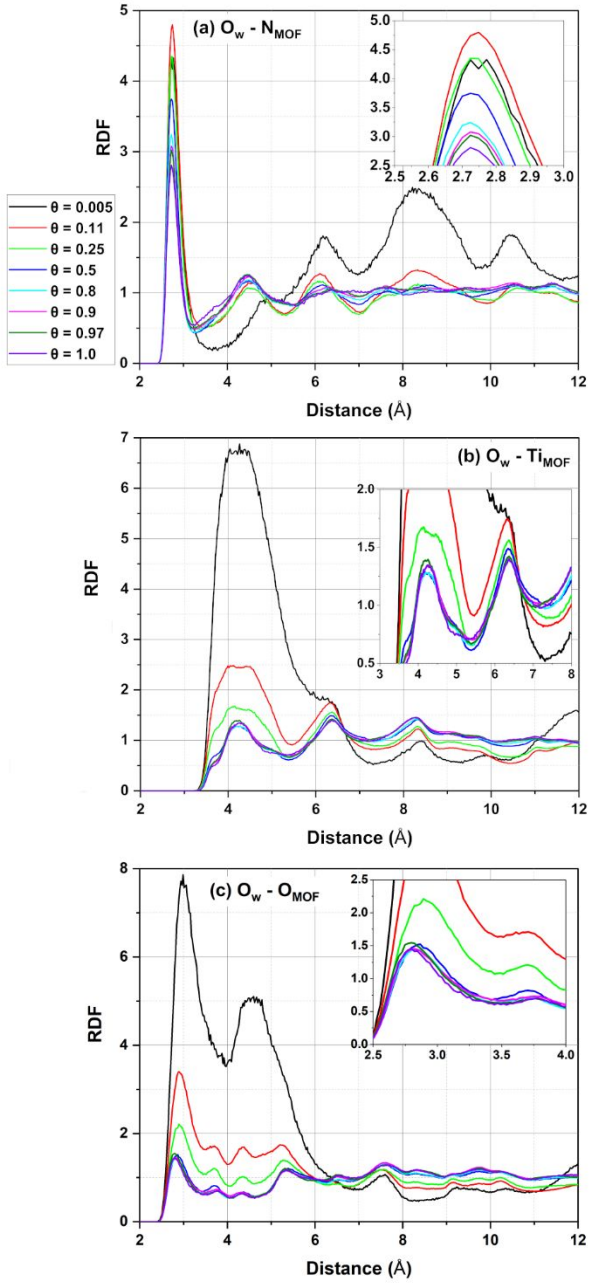

Figure 5. RDFs of three atomic pairs: oxygen of water with nitrogen of MOF (a), oxygen of water with

titanium of MOF (b), oxygen of water with oxygen of the hydroxyl groups of MOF (c). The insets show some additional details of the first peaks.

For the reported loadings, on the basis of the intensity of the first RDF peak, we could infer that nitrogen is the most attractive site for the oxygen of water, except at the lowest loading where the oxygen of the hydroxyl group seems to be the most attractive site. Therefore, from simulated RDFs, titanium and oxygen atoms, and the NH_2 group were identified as attractive sites for water, the latter being the most attractive one. This finding would explain the sensitivity of the ^{13}C chemical shift for the C-NH_2 carbon to the filling level,[22] and is consistent with the picture provided by the free energy analysis. The results of this analysis are depicted in Figure 6, where the focus is on a single large cage, shown on the left panel. The most favourable locations (shown as a system of green point clouds in the central panel of the figure) resulted to be close to, but not right at, the octamer window formed by titanium atoms and oxygens (although not right at the window), and close to the NH_2 moieties. The figure in the right panel shows the free energy landscapes within the pore. Specifically, the visualized lattice sites correspond to the plane cutting the cage of NH_2-MIL-125 in a direction perpendicular to y-axis in the middle of the titanium octamer window. The green regions indicate the most favourable locations (from -40 to -30 kJ/mol), the grey and blue regions indicate the least favourable locations (from -20 to 0 kJ/mol). The diffusional free energy barrier is associated with the molecule moving from the most favourable interaction sites to the interior of the pore, where interactions are weaker. Using the lattice percolation analysis, the minimum free energy pathway is identified and it yields a free energy barrier of about 20 kJ/mol.

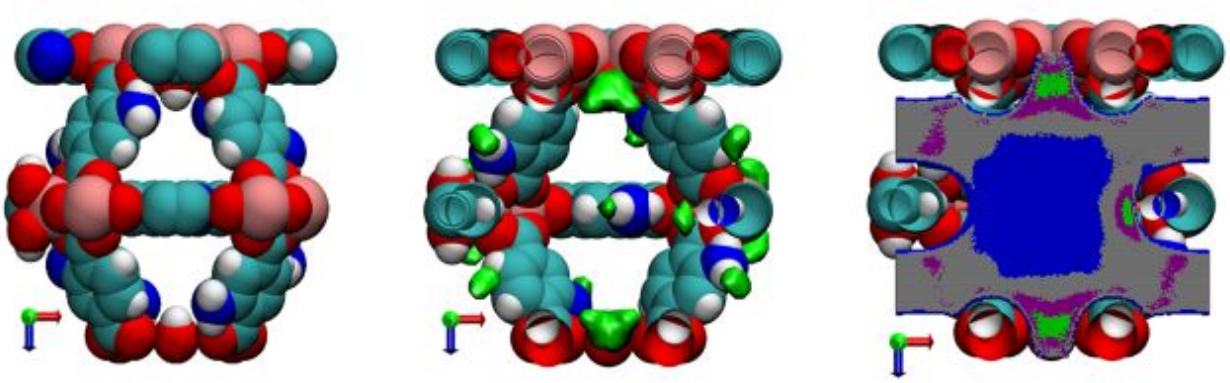

Figure 6. Free energy landscape analysis in NH_2-MIL-125. In the centre: most favourable interactions sites shown as green regions (from -40 to -30 kJ/mol). On the right: an x-z plane slicing through the centre of octamer Ti window. Colours represent the values of free energy: grey and blue from -20 to -10 and from -10 to 0 kJ/mol, respectively; purple from -30 to -20 kJ/mol; green from -40 to -30 kJ/mol. Colors for the atoms of the structure are as in Figure 1.

Water self-diffusivity and interaction energies from molecular simulations. MD simulations were also used to calculate the self-diffusivity of water in NH_2-MIL-125. To this end, the mean-squared displacements of the centre of mass of water molecules in the Fickian regime were collected. Self-diffusivity was then estimated using the Einstein equation (Eq. 11). MSDs of water diffusion for different loadings are shown in Figure 7, whereas the calculated self-diffusivity values are reported in Table 2. We note that at the very low loading (Figure 7a), the MSD shows a significant amount of scattering making the result invariably less reliable. The water self-diffusion coefficients determined from MD simulations were not strongly dependent on loading and assumed values around 10^{-10} m^2/s, with similar values at low and high loadings and a minimum at θ=0.08. This is not surprising, [48,49,50,51] since, at ambient temperatures, the diffusion of small molecules is normally retarded at very low

loadings due to strong interactions of adsorbate molecules with the framework. In contrast, at high loadings, where the pores are almost saturated, diffusion is hindered by the confining environment with little free space and adsorbate-adsorbate interactions dominate.

The self-diffusivity value of ~ 10^{-10} m^2/s is close to that experimentally measured for water in fully loaded MIL-100(Al),[6] Al-fumarate,[5] and MIL-96(Al).[7] Only in the case of MIL-100(Al), self-diffusivity was measured at different loadings and found to decrease by ~ 30 times at a filling factor of 0.2 compared to the value determined at full loading, which contrasts our MD data. The discrepancy may be due to the to the differences in nature of the inorganic and organic building blocks, pore size, pore window size and porous topology of MIL-100(Al) and NH_2-MIL-125. Water transport diffusivity was measured on NH_2-MIL-125 and a value of ~10^{-10} m^2/s was reported.[20] However, it must be noted that this is a transport diffusion coefficient, which is generally different from the self-diffusion coefficient.

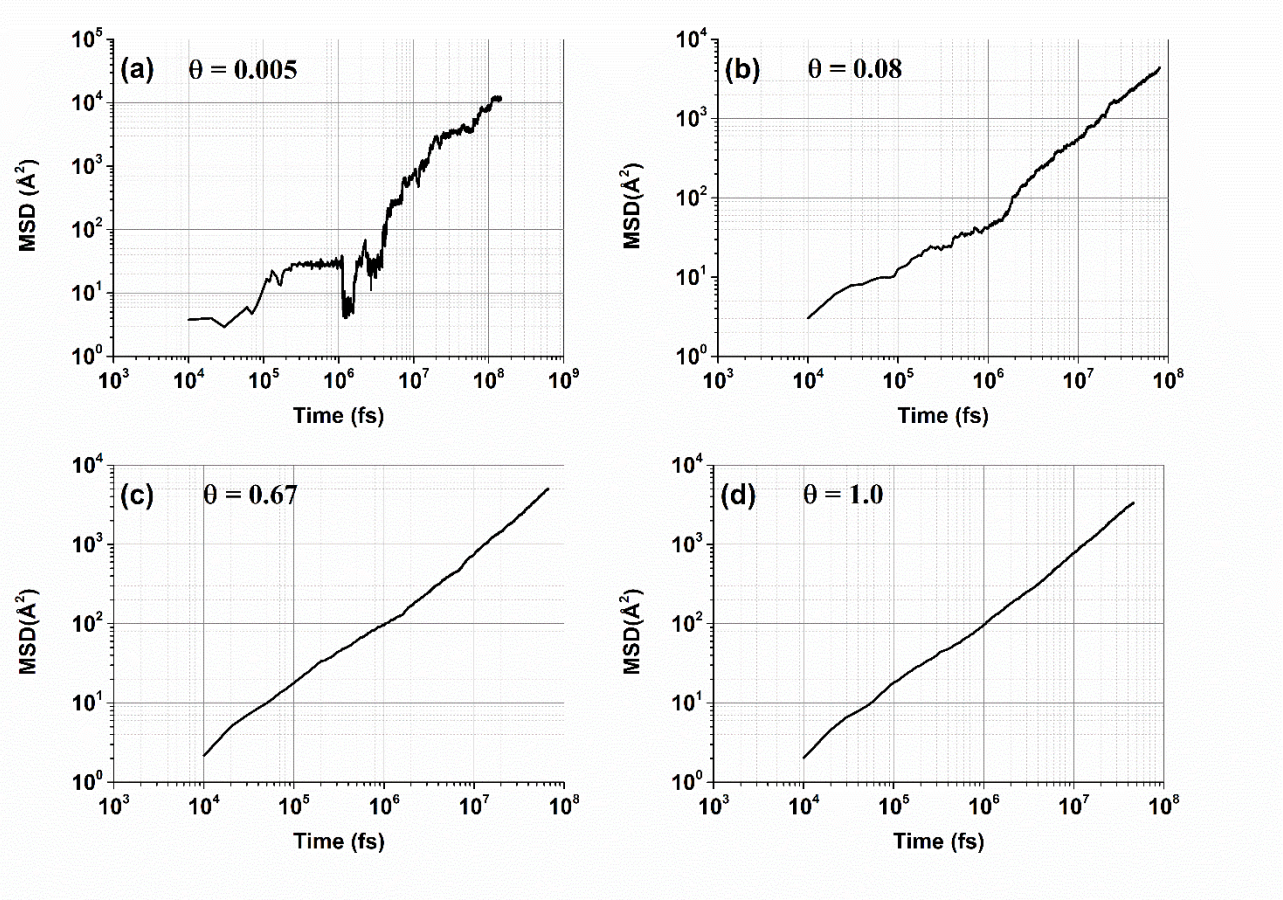

Figure 7. MSD of water in NH_2-MIL-125 as a function of time for selected relative loadings θ at 25 °C.

Table 2. Self-diffusion coefficients of water in NH_2-MIL-125 at different filling factors θ at 25 °C calculated using MD.

θ	D_{self} (m^2/s)	+/- Error
0.005	$1.47 \cdot 10^{-10}$	$8.35.10^{-11}$
0.08 (0.05 g/g)	$8.79 \cdot 10^{-11}$	$1.31.10^{-11}$
0.67 (0.4 g/g)	$1.25 \cdot 10^{-10}$	$7.67.10^{-12}$
1	$1.23 \cdot 10^{-10}$	$9.43.10^{-12}$

The dynamics of water in NH_2-MIL-125 from FFC NMR. The water dynamics in NH_2-MIL-125 was explored by ^{1}H FFC NMR at the pore-filling factor of 1. The signal detected was mainly due to water hydrogen atoms and to labile hydrogen atoms in the porous matrix participating to the hydrogen bond network of the water protons and contributing to the water signal through exchange on time scales shorter than 1 ms, as revealed by ^{1}H MAS spectra. Labile protons on porous matrices were found not to significantly affect T_1 of adsorbed water, as demonstrated in the case of the OH groups of Vycor, for which the dispersion curve of a monomolecular layer of adsorbed water did not significantly change when the OH groups were replaced by propoxy groups.[21] Similarly, the hydroxyl protons on residual methanol are expected to contribute to the detected water signal because of rapid exchange. On the other hand, the aromatic protons of the matrix were supposed not to significantly contribute to the observed R_1 values. In fact, spin diffusion between the water protons and the aromatic ones is likely to be ineffective because of the mobility of the surface phase, with the result that the minor fast decaying signal from the aromatic protons is undetectable due to instrumental limitations (essentially, relatively long dead time).

^{1}H FFC NMR relaxometry allows molecular dynamics to be investigated by measuring the dependence of the proton spin–lattice relaxation rate R_1 on the Larmor frequency, ν_0. Schematically, in the R_1 *vs* ν_0 curve the occurrence of a dynamic process characterized by a given correlation time, τ_c, manifests itself as a flat region when $2\pi\nu_0 \ll 1/\tau_c$, that is, at the low Larmor frequency side, and a region where the relaxation rate R_1 decreases with increasing frequency with a dispersion centered at $2\pi\nu_0 \approx 1/\tau_c$.[52]

The dispersion profiles measured at temperatures ranging between 25 and 80 °C are shown in Figure 8. The ^{1}H R_1 values were much larger than the typical values for bulk water at ambient temperature and at the same Larmor frequencies, roughly 0.3 s^{-1} and frequency independent; the values obtained are indeed typical of confined water. Close inspection of the data suggested that two dispersions occurred, a barely discernible one centered at 3-4 MHz and a more pronounced one around 0.1 MHz, indicating the

presence of at least two dynamic processes. The first dispersion did not visibly change upon heating, whereas the second one tended to shift to lower R_1 values (Figure 8a). This suggests that the underlying dynamic process was accelerating. A third process was also present, as evidenced by the high frequency plateau. This was ascribed to a local motion, too fast to show a dispersion inside the observed frequency window and identified with the isotropic rotation of water and of the methyl group of residual methanol. Also self-diffusion, which however was not taken in account here due to its negligible value, would contribute to this high frequency plateau.

Numerical analysis of the data provided the fitting curves associated to each process, also displayed in Figure 8. The low-frequency dispersion was interpreted according to the RMTD model, [21] as described in the Materials and Methods section. The RMTD model considers that water molecules close to the pore surface hop among preferential binding sites and are reoriented as a consequence of the displacements along the surface. Such molecular reorientations occur on a much slower time scale than in the bulk. The RMTD contribution to R_1 depends on the weight factor A_{RMTD} (Eq. 7), and on the largest and smallest cut-off frequencies, $\nu_{RMTD,max}$ and $\nu_{RMTD,min}$, characterizing the faster and slower reorientations mediated by translational diffusion on the surface (Eqs. 5 and 6).

The high-frequency dispersion was interpreted as due to restricted reorientations of bound water molecules, the presence of which was highlighted by ^{1}H MAS.

The best fitting parameters reproducing the experimental curves are reported in Table 3 and their temperature dependence is plotted in Figure 9.

The correlation time of restricted reorientation, τ_{RR}, is about 30 ns and exhibits an Arrhenius temperature dependence characterized by a relatively small activation energy of 4.5 kJ/mol (Figure 9d, $ln(\tau_{RR}) \propto \frac{activation\ energy}{RT}$, where R indicates the gas constant). This value is significantly different from that exhibited by reorientation in bulk water, which is equal to 15-16 kJ/mol as derived after Arrhenius

fits of published data.[53,54] Indeed, it seems reasonable that the energy of the interactions involved in the restricted reorientation is lower than that associated to a full reorientation like the one occurring in bulk, where more bonds are likely to be broken.

The parameters $\nu_{RMTD,min}$ and $\nu_{RMTD,max}$ show Arrhenius dependencies, with activation energies of 15 ± 1 kJ/mol and 18 ± 4 kJ/mol, respectively (Figures 9b and 9c). These values are not different within the experimental error, suggesting that their temperature dependences are dominated by that of the surface diffusion parameter, D ($ln(D) \propto -\frac{activation\ energy}{RT}$). In fact, this is expected on the basis of Eqs. 5 and 6, considering that q, identifying a diffusion mode, is related to the surface structure and independent of temperature.

The temperature dependence of $1/A_{RMTD}^2$ is also Arrhenius-like and characterized by an activation energy of 15 ± 1 kJ/mol (Figure 9a), a value equal to those exhibited by $\nu_{RMTD,min}$ and $\nu_{RMTD,max}$ within the experimental error. For A_{RMTD}, besides D also the fraction of bound molecules, p_b, and the order parameter, S, in principle affect its temperature dependence (Eq. 7). However, the observed A_{RMTD} temperature dependence, when compared to those of $\nu_{RMTD,min}$ and $\nu_{RMTD,max}$, indicated that p_b and S did not change significantly in the explored temperature range. This fact is in agreement with the very small decrease of the water side bands intensity in the NMR spectra upon heating. An activation energy of 16 ± 2 kJ/mol relative to D was derived as an average of the values determined for each fitting parameter. This value is consistent with the free energy analysis of the binding sites and the barriers between them. In fact, the free energy analysis of the porous space identified the transition from favorable binding sites (near titanium rings and the NH_2 group) to non-bonded states close to the surface as the key energy barrier and estimated its value at about 20 kJ/mol, which is in a good agreement with the experimental interpretation above. Surface diffusion is expected to be an activated process because it depends on the breaking of the binding of the molecules to the surface before

hopping. One can also notice that the value of the activation energy favorably compares with that observed for diffusion in bulk water, 16.8 ± 0.1 kJ/mol, as derived after an Arrhenius fit of published experimental diffusion coefficient values in the temperature interval 25-80 °C.[55] This indicates that the energy of the interactions involved in the detachment of a water molecule from a binding site in completely filled cages is not significantly different from that driving bulk diffusion.

The insignificant change of p_b and S is in agreement with the fact that the prefactor for the restricted reorientation, $Kp_b(1-S^2)$, did not significantly change with temperature. On the other hand, p_bS^2 could be evaluated from the best fit values of A_{RMTD}, $\nu_{RMTD,max}$ and $\nu_{RMTD,min}$ to an average value of 0.096±0.005. Using these constraints, the values of p_b and S were estimated to be ~ 0.2 and ~0.7, respectively. The estimated p_b can be compared with that derived considering the number of plausible binding sites available per water molecule in the completely loaded sample. In a $Ti_8O_8(OH)_4(NH_2BDC)_6$ unit, if the binding sites are the amine and Ti-OH-Ti hydroxyl groups of the matrix, as hinted by MD simulations and ^{13}C NMR spectra,[22] and 40 water molecules occupy the empty space according to the NMR calibration, the value of p_b would result to be 0.25. The values of p_b from the two estimates are grossly comparable. A possible reason for the slight discrepancy is the underestimation of the bound fraction because of its lower detectability due to the instrumental dead time and poor magnetic field homogeneity.

Using the determined values of p_b, we estimated the value of isotropic reorientation time, τ_{IR}, from the high frequency plateau value and found about 0.4 ns. Since also the fast rotation about the C3 axis of the methyl group of residual methanol is likely to contribute to the plateau value, the estimate of 0.4 ns should be considered as an upper limit for τ_{IR} of water.

From the model fitting it was also possible to evaluate the minimum and maximum distances, l_{min} and l_{max}, travelled by water molecules within the RMTD model before losing orientational correlation. These distances were derived from the fitted $\nu_{RMTD,min}$ and $\nu_{RMTD,max}$ values at 25 °C using Eqs. 8 and

9, with the surface diffusion coefficient D set equal to $1.23 \cdot 10^{-10}$ m^2/s, *i. e.,* the self-diffusion coefficient determined through the MD simulations at θ=1. The estimated l_{min} and l_{max} values are 40 ± 8 Å and 850 ± 150 Å, respectively. l_{min} favorably compares to the larger pore circumference of ~35 Å, whereas l_{max} is on the order of the crystallite size, for which the lower bound of 450 Å was determined from the line width of the XRD pattern exhibited by dry NH_2-MIL-125 [18] using Scherrer's equation.

Table 3. Parameters used to fit the experimental curves.[a]

T (°C)	A_{RMTD} ($s^{1/2}$)	$\nu_{RMTD,min}$ (Hz)	$\nu_{RMTD,max}$ (Hz)	τ_{RR} (ns)
25	$(3.54 \pm 0.20) \cdot 10^{-6}$	$(1.1 \pm 0.4) \cdot 10^4$	$(5 \pm 2) \cdot 10^6$	31 ± 3
30	$(3.27 \pm 0.20) \cdot 10^{-6}$	$(1.1 \pm 0.4) \cdot 10^4$	$(5 \pm 2) \cdot 10^6$	31 ± 3
40	$(3.00 \pm 0.20) \cdot 10^{-6}$	$(1.3 \pm 0.4) \cdot 10^4$	$(6 \pm 2) \cdot 10^6$	27 ± 3
50	$(2.65 \pm 0.20) \cdot 10^{-6}$	$(1.8 \pm 0.4) \cdot 10^4$	$(9 \pm 4) \cdot 10^6$	26 ± 2
60	$(2.42 \pm 0.20) \cdot 10^{-6}$	$(1.9 \pm 0.4) \cdot 10^4$	$(8 \pm 2) \cdot 10^6$	25 ± 2
70	$(2.29 \pm 0.20) \cdot 10^{-6}$	$(2.3 \pm 0.4) \cdot 10^4$	$(11 \pm 4) \cdot 10^6$	24 ± 2
80	$(2.36 \pm 0.20) \cdot 10^{-6}$	$(2.7 \pm 0.4) \cdot 10^4$	$(20 \pm 10) \cdot 10^6$	24 ± 2

[a] The prefactor for the restricted reorientation, $Kp_b(1 - S^2)$, was $6.6 \cdot 10^8$ s^{-2} at all the temperatures and τ_{IR}=0.4 ns.

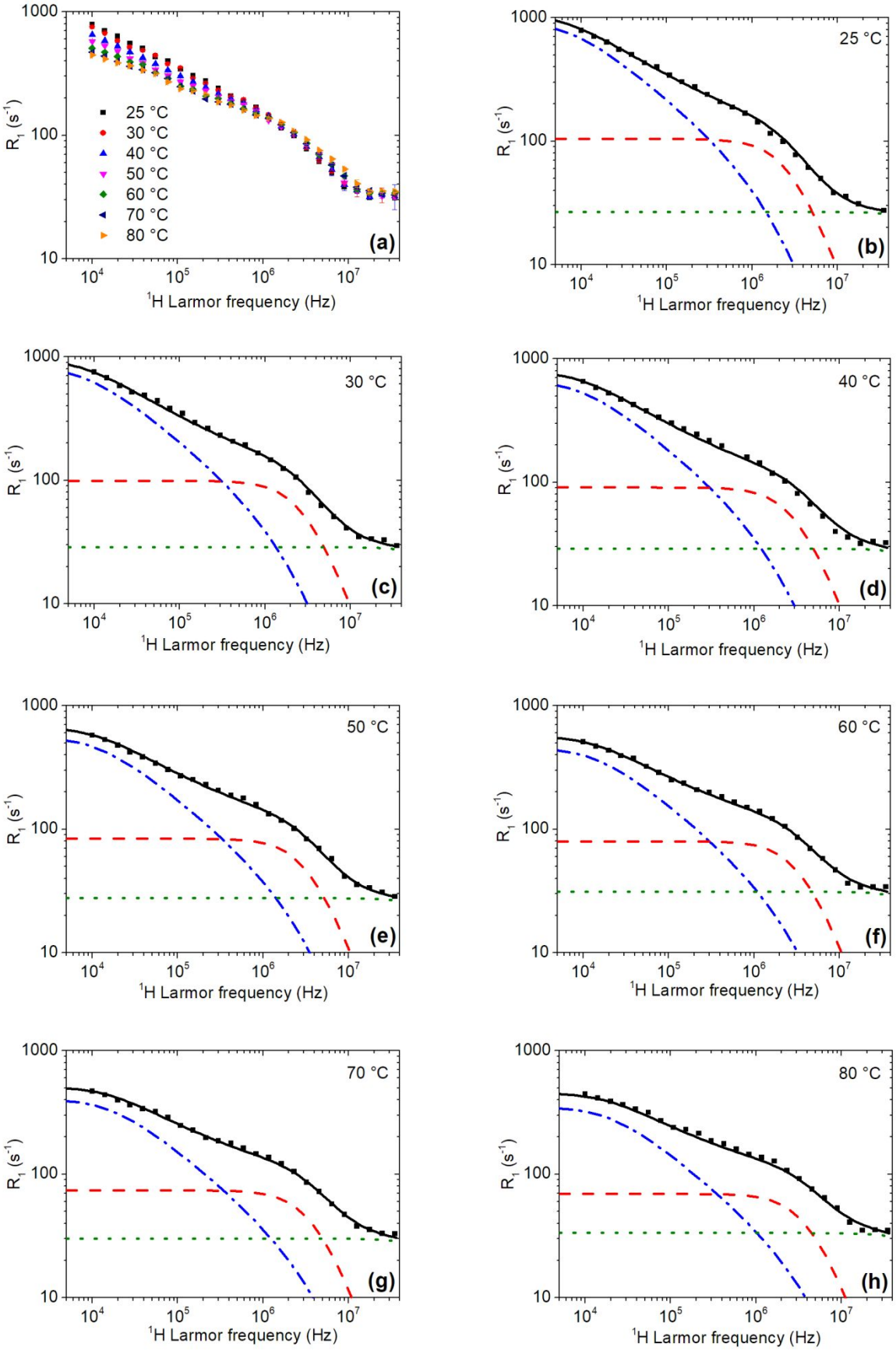
25 °C
30 °C
40 °C
50 °C
60 °C
70 °C
80 °C
(a)
(b)
(c)
(d)
(e)
(f)
(g)
(h)
R1 (s-1)
1H Larmor frequency (Hz)

Figure 8. (a) Experimental R_1 NMRD curves of completely hydrated NH_2-MIL-125 at the indicated temperatures. (b)-(h) Comparison of the experimental (squares) and calculated (black line) R_1 NMRD curves at each temperature. Blue dash-dotted, red dashed, and green dotted lines represent contributions to R_1 from RMTD mechanism, anisotropic and isotropic rotational dynamics, respectively.

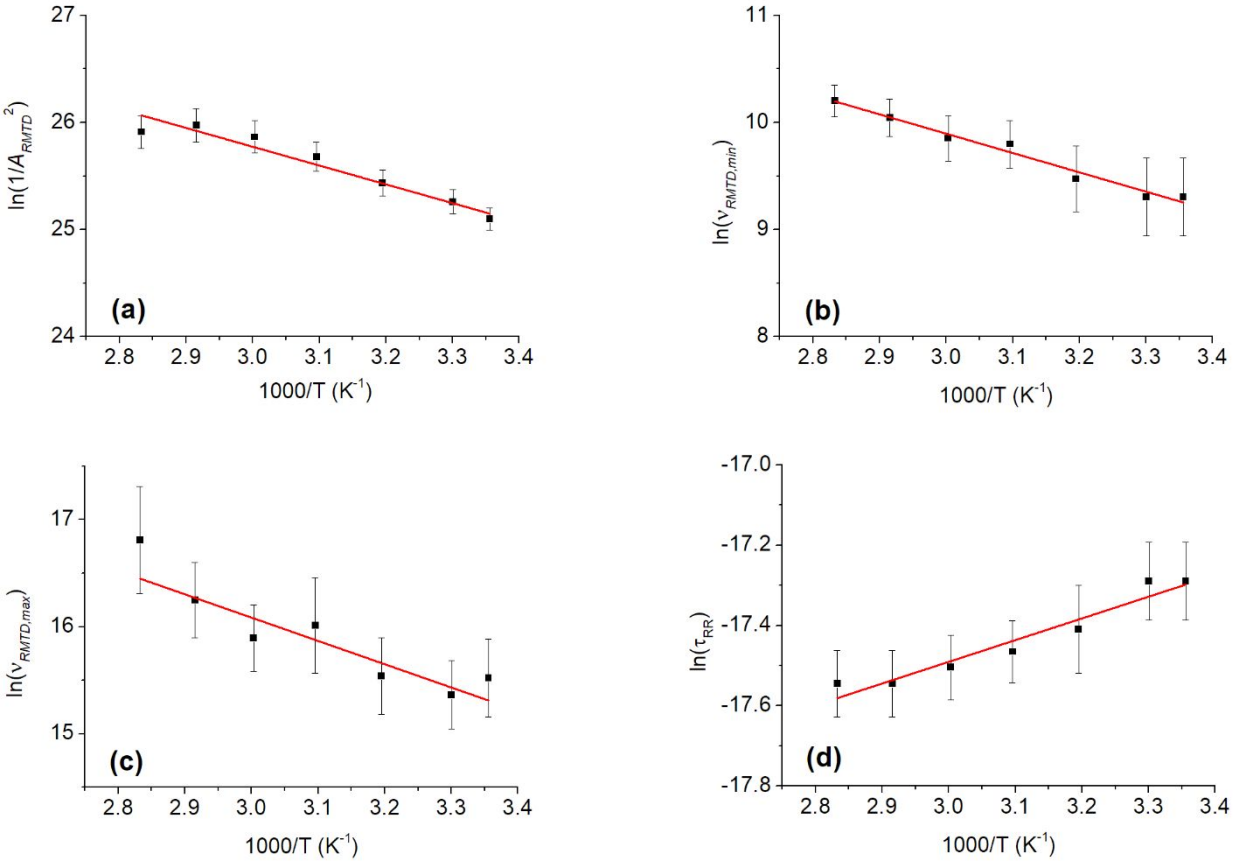

Figure 9. Temperature trend of the fitting parameters $1/A_{RMTD}^2$, $\nu_{RMTD,min}$, $\nu_{RMTD,max}$, and τ_{RR} in panels a, b, c, and d, respectively). The straight red lines represent Arrhenius fits with activation energies of 15 ± 1 kJ/mol, 15 ± 1 kJ/mol, 18 ± 4 kJ/mol, and 4.5 ± 0.5 kJ/mol for panel a, b, c, and d, respectively.

Conclusions

To the best of our knowledge, this is the first time that ^{1}H FFC NMR relaxometry was applied to study the dynamics of a guest molecule in a metal organic framework. A coherent picture of water motions in NH_2-MIL-125 was provided in the time scale 10 μs - 0.1 ns in the temperature range 25-80 °C. The FFC NMR data were interpreted using a dynamic model developed for molecules in porous media, whose applicability to the present case was supported by independent ^{1}H MAS measurements and by molecular simulations.

The model depends on physically meaningful parameters characterized by rationalized temperature trends. It allowed a detailed picture of the behavior of water molecules within the MOF pores to be obtained. In the fully hydrated NH_2-MIL-125 MOF, a small fraction (about 20%) of water molecules hops among preferential binding sites and is reoriented as a consequence of the displacement along the surface. This motion occurs on a very broad time scale ranging from several nanoseconds to a few microseconds. The bound water molecules also experience local restricted molecular reorientations with characteristic times of about 30 ns, whereas free water molecules exhibit isotropic correlation times shorter than 0.4 ns. The temperature dependence of the hopping rate indicates that the process is thermally activated, with an Arrhenius-like dependence characterized by an activation energy of 16 ± 2 kJ/mol. This value matches the energy barrier between favorable binding sites and non-bonded states close to the surface, as evaluated from free energy analysis. The plausibility of the analysis could also be tested with regard to the length scales of the system. The minimum and maximum distances associated to water correlated reorientations on the porous surface are comparable with the diameter of the larger pores and the crystal size, respectively.

Besides the dynamic details obtained, this study demonstrates the applicability and usefulness of FFC NMR, so far applied to aqueous solutions, soft matter or fluids in disordered porous materials, also in

the case of fluids in MOFs, disclosing information of relevance for their technological application. It also testifies that computational approaches valuably complement the FFC NMR experimental tool to characterize the diffusion behaviour of a small molecule in a MOF and are invaluable in the rationalization of its adsorption properties.

Acknowledgements

SP and CF would like to acknowledge the contribution of the COST Action CA15209 (Eurelax: European Network on NMR Relaxometry). LS would like to thank Prof. Guillaume Maurin for the simulation-ready cif file for NH_2-MIL-125 and other useful comments.

Supporting Information. Complete set of properties calculated by Poreblazer; description of the input and output files within Poreblazer v4.0: structure of the input.dat file (Table S1), structure of the defaults.dat file (Table S2), fragment of the UFF.atoms file (Table S3), results in summary.dat file (Table S4), additional files (Table S5); details on the methods employed to explore binding sites within NH_2-MIL-125 and free energy barriers for water molecules within NH_2-MIL-125; GCMC simulated adsorption isotherm of water on NH_2-MIL-125 compared to experimental data measured at 298 K (Figure S1a) and enthalpy of adsorption for the simulated isotherm at 298 K (Figure S1b); variation of water-water and water-MOF interactions as a function of relative water pressure obtained from the GCMC simulations (Figure S2); variation of water-water and water-MOF van der Waals and coulombic interactions as a function of pressure from GCMC simulations (Figure S3); molecular visualization of water molecules in cages of NH_2-MIL-125 (Figure S4); details on the identification and quantification of residual solvent using ^{13}C solid state NMR; ^{13}C direct excitation spectrum of NH_2-

MIL-125 at the filling factor 0.09 (Figure S5); $^{13}C/^{1}H$ correlation spectrum of NH_2-MIL-125 at the filling factor 0.09 (Figure S6) (PDF).

References

(1) Kimmich, R. *Principles of Soft-Matter Dynamics, Basic Theories, Non-invasive Methods, Mesoscopic Aspects*; Springer Science+Business Media: Dordrecht, The Netherlands, 2012.

(2) Maurin, G. Role of Molecular Simulations in the Field of MOFs In: *The Chemistry of Metal–Organic Frameworks,* chap. 25, 2016 Wiley-VCH Verlag GmbH & Co. KGaA, Boschstr. 12, 69469 Weinheim, Germany.

(3) Pizzanelli, S.; Monti, S.; Gordeeva, L. G.; Solovyeva, M. V.; Freni, A.; Forte, C. A Close View to the Organic Linker in a MOF: Structural Insights from a Combined ^{1}H NMR Relaxometry and Computational Investigation. *Phys. Chem. Chem. Phys.* **2020,** *22,* 15222-15230.

(4) Stallmach, F.; Gröger, Künzel, V.; Kärger, J.; Yaghi, O. M.; Hesse, M.; Müller, U. NMR Studies on the Diffusion of Hydrocarbons on the Metal-Organic Framework Material MOF-5. *Angew. Chem. Int. Ed.* **2006,** *45,* 2123-2126.

(5) Splith, T.; Frölich, D.; Henninger, S. K.; Stallmach, F. Development and Application of an Exchange Model for Anisotropic Water Diffusion in the Microporous MOF Aluminum Fumarate. *J. Magn. Reson.* **2018,** *291,* 40-46.

(6) Splith, T.; Pantatosaki, E.; Kolokathis, P. D.; Fröhlich, D.; Zhang, K.; Fülder, G.; Chmelik, C.; Jiang, J.; Henninger, S. K.; Stallmach, F.; *et al*. Moleular Dynamics Phenomena of Water in the Metalorganic Framework MIL-100(Al), as Revealed by Pulsed Field Gradient NMR and Atomistic Simulation. *J. Phys. Chem. C* **2017,** *121,* 18065-18074.

(7) Velasco, M. I.; Acosta R. H.; Marmisollé, W. A.; Azzaroni, O.; Rafti, M. Modulation of Hydrophilic/Hydrophobic Character of Porous Environments in Metal-Organic Frameworks via Direct Polymer Capping Probed by NMR Diffusion Measurements. *J. Phys. Chem. C* **2019,** *123,* 21076-21082.

(8) Thoma, R.; Kärger, J.; de Sousa Amadeu, N.; Nießing, S.; Janiak, C. Assessing Guest-Molecule Diffusion in Heterogeneous Powder Samples of Metal-Organic Frameworks through Pulsed-Field-Gradient (PFG) NMR Spectroscopy. *Chem. Eur. J.* **2017,** *23,* 13000-13005.

(9) Bermúdez-García, J. M.; Vicent-Luna, J. M.; Yañez-Vilar, S.; Hamad, S.; Sánchez-Andújar, M.; Castro-García, S.; Calero, S.; Señaris-Rodríguez, M. A. Liquid Self-diffusion of H_2O and DMF Molecules in Co-MOF-74: Molecular Dynamics Simulations and Dielectric Spectroscopy Studies. *Phys. Chem. Chem. Phys.* **2016,** *18,* 19605-19612.

(10) Skarmoutsos, I.; Eddaoudi, M.; Maurin, G. Highly Efficient Rare-Earth Metal Organic Frameworks for Water Adsorption: A Molecular Modeling Approach. *J. Phys. Chem. C* **2019,** *123,* 26989-26999.

(11) Medders, G. R.; Paesani, F. Water Dynamics in Metal-Organic Frameworks: Effects of Heterogeneous Confinement Predicted by Computational Spectroscopy. *J. Phys. Chem. Lett.* **2014,** *5,* 2897-2902.

(12) Salles, F.; Bourrelly, S.; Jobic, H.; Devic, V.; Guillerm, V.; Llewellyn, P.; Serre, C.; Ferey, G.; Maurin, G. Molecular Insight into the Adsorption and Diffusion of Water in the Versatile Hydrophylic/Hydrophobic Flexible MIL-53(Cr) MOF. *J. Phys. Chem. C* **2011,** *115,* 10764-10776.

(13) Bendt, S.; Dong, Y.; Keil, F. J. Diffusion of Water and Carbon Dioxide and Mixtures Thereof in Mg-MOF-74. *J. Phys. Chem. C* **2019,** *123,* 8212-8220.

(14) Paesani, F. Water in Metal-Organic Frameworks: Structure and Diffusion of H_2O in MIL-53(Cr) from Quantum Simulations. *Mol. Simul.* **2012,** *38,* 631-641.

(15) Terranova, Z. L.; Agee, M. M.; Paesani, F. Water Structure and Dynamics in Homochiral [Zn(*I*-L)(X)] Metal-Organic Frameworks. *J. Phys. Chem. C* **2015,** *119,* 18239-18247.

(16) Haigis, V.; Coudert, F.-X; Vuilleumier, R.; Boutin A. Investigation of Structure and Dynamics of the Hydrated Metal-Organic Framework MIL-53(Cr) Using First-Principles Molecular Dynamics. *Phys. Chem. Chem. Phys.* **2013,** *15,* 19049-19056.

(17) Jeremias, F.; Lozan, V.; Henninger, S.K.; Janiak C. Programming MOFs for Water Sorption: Aminofunctionalized MIL-125 and UiO-66 for Heat Transformation and Heat Storage Applications. *Dalton Trans.* **2013,** *42,* 15967-15973.

(18) Gordeeva, L. G.; Solovyeva, M. V.; Aristov, Y. I. NH_2-MIL-125 as a Promising Material for Adsorptive Heat Transformation and Storage. *Energy* **2016,** *100,* 18-24.

(19) Solovyeva, M. V.; Aristov, Y. I.; Gordeeva, L. G. NH_2-MIL-125 as a Promising Adsorbent for Adsorptive Cooling: Water Adsorption Dynamics. *Appl. Therm. Eng.* **2017,** *116,* 541-548.

(20) Graf S.; Redder, F.; Bau, U.; de Lange, M.; Kapteijn, F.; Bardow, A. Toward Optimal Metal–Organic Frameworks for Adsorption Chillers: Insights from the Scale-Up of MIL-101(Cr) and NH_2-MIL-125. *Energy Technol.* **2020,** *8,* 1900617.

(21) Stapf, S.; Kimmich, R.; Niess, J. Microstructure of Porous Media and Field-Cycling Nuclear Magnetic Relaxation Spectroscopy. *J. Appl. Phys.* **1994,** *75,* 529-537.

(22) Pizzanelli, S.; Freni, A.; Forte, C. Water Modulated Framework Flexibility in NH_2-MIL-125: Highlights from ^{13}C Nuclear Magnetic Resonance. *Heat Transfer Eng.* **2022,** *43,* in press.

(23) Abragam A. *Principles of Nuclear Magnetism;* Oxford University Press: Oxford, UK, 1983.

(24) Rabideau, S. W.; Finch, E. D.; Denison, A. B. Proton and Deuteron NMR of Ice Polymorphs. *J. Chem. Phys.* **1968,** *49,* 4660-4665.

(25) Sebastião, P. J.; Sousa, D.; Ribeiro, A. C.; Vilfan, N.; Lahajnar, G.; Seliger, J.; Žumer, S. Field-cycling NMR Relaxometry of a Liquid Crystal Above T_{NI} in Mesoscopic Confinement. *Phys. Rev. E* **2005,** *72,* 061702.

(26) Stapf, S.; Kimmich, R.; Seitter, R.-O. Proton and Deuteron Field-Cycling NMR Relaxometry of Liquids in Porous Glasses: Evidence for Levy-Walk Statistics. *Phys. Rev. Lett.* **1995,** *75,* 2855-2858.

(27) Carvalho, A.; Sebastião, P. J; Fonseca, I.; Matos, J.; Gonçalves, M. C. Silica and Silica Organically Modified Nanoparticles: Water Dynamics in Complex Systems. *Microporous Mesoporous Mater.* **2015,** *217,* 102-108.

(28) Bloembergen, N.; Purcell, E. M.; Pound, R. V. Relaxation Effects in Nuclear Magnetic Resonance Absorytion. *Phys. Rev.* **1948,** *73,* 679-712.

(29) Torrey, H. C. Nuclear Spin Relaxation by Translational Diffusion. *Phys. Rev.* **1953,** *92,* 962-969.

(30) Harmon, J. F.; Muller, B. H. Nuclear Spin Relaxation by Translational Diffusion in Liquid Ethane. *Phys. Rev.* **1969,** *182,* 400-410.

(31) P. J. Sebastião, Fitteia. Fitting Environment Interfaces for All. http://fitteia.org (date last accessed: February 2, 2021).

(32) Sebastião, P. J. The Art of Model Fitting to Experimental Results. *Eur. J. Phys.* **2014,** *35,* 015017.

(33) Vaesen, S.; Guillerm, V.; Yang, Q.; Wiersum, A. D.; Marszalek, B.; Gil, B.; Vimont, A.; Daturi, M.; Devic, T.; Llewellyn, P. L.; *et al*. A Robust Amino-Functionalized Titanium(iv) Based MOF for Improved Separation of Acid Gases. *Chem. Comm.* **2013,** 49, 10082-10084.

(34) Sarkisov, L. Calculation and Visualization of Free Energy Barriers for Several VOCs and TNT in HKUST-1. *Phys. Chem. Chem. Phys.* **2012,** *14,* 15438-15444.

(35) Sarkisov, L. Toward Rational Design of Metal–organic Frameworks for Sensing Applications: Efficient Calculation of Adsorption Characteristics in Zero Loading Regime. *J. Phys. Chem. C* **2012,** *116,* 3025-3033.

(36) Dubbeldam, D.; Calero, S.; Ellis, D. E.; Snurr, R. Q. RASPA: Molecular Simulation Software for Adsorption and Diffusion in Flexible Nanoporous Materials. *Mol. Simul.* **2016,** *42,* 81-101.

(37) Abascal, J. L. F.; Vega, C. A General Purpose Model for the Condensed Phases of Water: TIP4P/2005. *J. Chem. Phys.* **2005,** 123, 234505.

(38) Torres-Knoop, A.; Poursaeidesfahani, A.; Vlugt, T. J. H.; Dubbeldam, D. Behavior of the Enthalpy of Adsorption in Nanoporous Materials Close to Saturation Conditions. *J. Chem. Theory Comput.* **2017,** 13, 3326-3339.

(39) Plimpton, S. Fast Parallel Algorithms for Short-Range Molecular Dynamics. *J. Comput. Phys.* **1995,** *117*, 1-19.

(40) Hoover, W. G. Canonical Dynamics: Equilibrium Phase-Space Distributions. *Phys. Rev. A* **1985,** *31,* 1695-1697.

(41) Martyna, G. J.; Tuckerman, M. E.; Tobias, D. J.; Klein, M. L. Explicit Reversible Integrators for Extended Systems Dynamics. *Mol. Phys.* **1996,** *87,* 1117-1157.

(42) Martyna, G. J.; Klein, M. L.; Tuckerman, M. Nosé–Hoover chains: The Canonical Ensemble Via Continuous Dynamics. *J. Chem. Phys.* **1992,** *97,* 2635-2643.

(43) Hockney, R. W.; Eastwood, J. W. *Computer Simulation Using Particles*. Institute of Physics Publishing: New York, 1989; p 540.

(44) ten Elshof, J. E.; Abadal, C. R.; Sekulić, J.; Chowdhury, S. R.; Blank, D. H. A. Transport Mechanisms of Water and Organic Solvents Through Microporous Silica in the Pervaporation of Binary Liquids. *Microporous Mesoporous Mater.* **2003,** *65,* 197–208.

(45) Devautour-Vinot, S.; Maurin, G.; Serre, C.; Horcajada, P.; da Cunha, D. P.; Guillerm, V.; de Souza Costa, E.; Taulelle, F.; Martineau, C. Structure and Dynamics of the Functionalized MOF Type UiO-66(Zr): NMR and Dielectric Relaxation Spectroscopies Coupled with DFT Calculations. *Chem. Mater.* **2012,** *24,* 2168−2177.

(46) Chary, Komandur V. R.; Bhaskar, T.; Kishan, G.; Vijayakumar, V. Characterization of MoO3/TiO2 (Anatase) Catalysts by ESR, ^{1}H MAS NMR, and Oxygen Chemisorption. *J. Phys. Chem. B* **1998,** *102,* 3936-3940.

(47) Naito, A.; Root, A.; McDowell C. A. Combined Sample Rotation and Multiple-Pulse NMR Spectroscopic Studies on Protons Bonded to ^{14}N Nuclei in Solid Amino Acids. *J. Phys. Chem.* **1991,** *95,* 3578-3581.

(48) Brandani, S.; Ruthven, D. M.; Kärger, J. Concentration Dependence of Self-Diffusivity of Methanol in NaX Zeolite Crystals. *Zeolites* **1995,** *15*, 494-495.

(49) Valiullin, R.; Kärger, J.; Gläser, R. Correlating Phase Behaviour and Diffusion in Mesopores: Perspectives Revealed by Pulsed Field Gradient NMR. *Phys. Chem. Chem. Phys.* **2009,** *11*, 2833-2853.

(50) Mera, H. A.; Gomez-Ballesteros, J. L.; Balbuena, P. B. Structure and Dynamics of Carbon Dioxide, Nitrogen, Water, and Their Mixtures in Metal Organic Frameworks. *J. Chem. Eng. Data* **2014,** *59*, 2973-2981.

(51) Farmahini, A. H.; Shahtalebi, A.; Jobic, H.; Bhatia, S. K. Influence of Structural Heterogeneity on Diffusion of CH_4 and CO_2 in Silicon Carbide-Derived Nanoporous Carbon. *J. Phys. Chem. C* **2014,** *118*, 11784-11798.

(52) Kimmich, R.; Anoardo, E. Field-cycling NMR Relaxometry. *Prog. Nucl. Magn. Reson. Spectrosc.* **2004,** 44, 257-320.

(53) Ludwig, R.; Weinhold, F.; Farrar, T. C. Experimental and Theoretical Determination of the Temperature Dependence of Deuteron and Oxygen Quadrupole Coupling Constants of Liquid Water. *J. Chem. Phys.* **1995,** *103,* 6941-6950.

(54) Cho, C. H.; Urquidi, J.; Singh, S.; Wilse Robinson, G. Thermal Offset Viscosities of Liquid H_2O, D_2O, and T_2O. *J. Phys. Chem. B* **1999,** *103,* 1991-1994.

(55) Holz M.; Heil, S. R.; Sacco, A. Temperature-dependent Self-diffusion Coefficients of Water and Six Selected Molecular Liquids for Calibration in Accurate ^{1}H NMR PFG Measurements. *Phys. Chem. Chem. Phys.* **2000,** *2,* 4740-4742.

Table of Contents

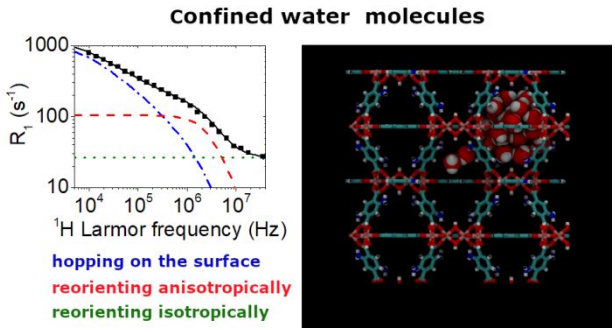

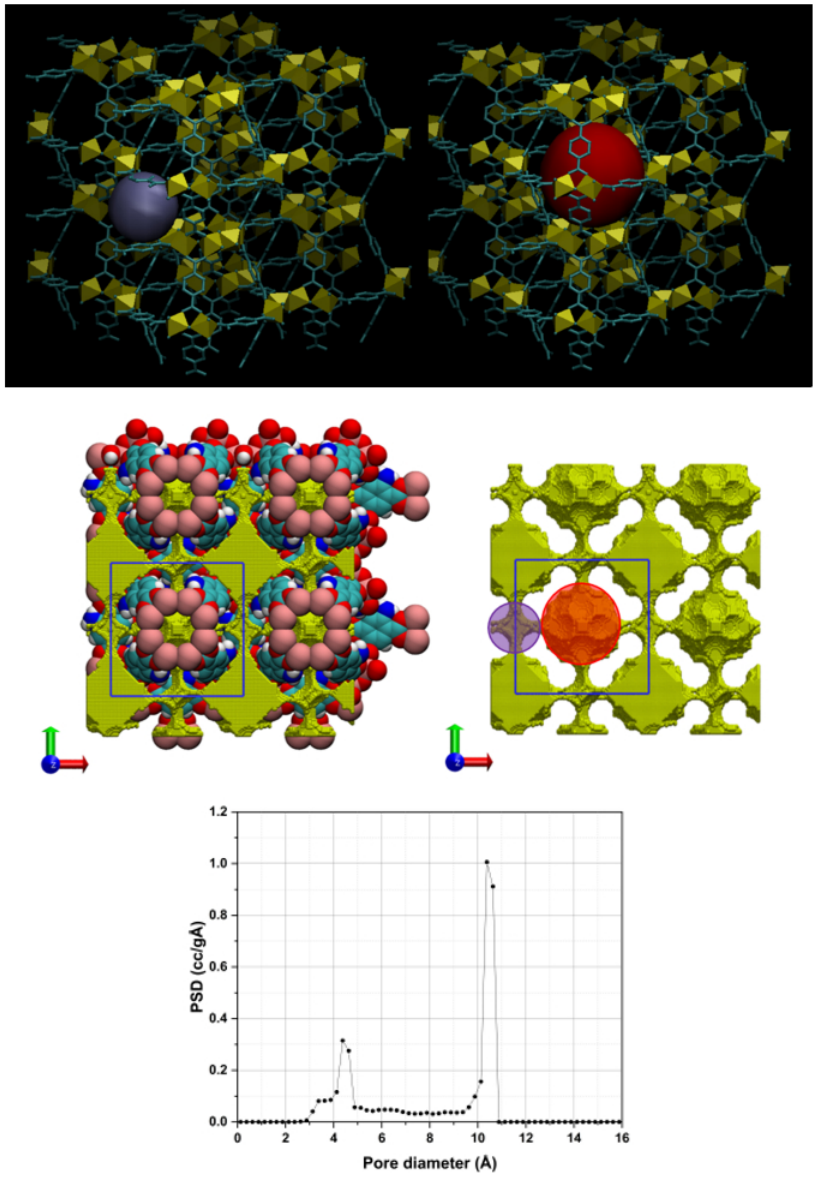

Figure 1. Structural characterization of NH_2-MIL-125. Top panel: the NH_2-MIL-125 is shown as cyan bond framework and yellow tetrahedra Ti-O units. The two main pores in the system are shown as encapsulated red (10.65 Å) and purple (4.5 Å) spheres. Middle panel: the structural organization of the pore network in NH_2-MIL-125 is shown as lattice of available sites (yellow). The network consists of intercalating small and large pores, connected by narrow windows. The pores identified in the top panel, are shown in this figure as red and purple circles. A single unit cell of NH_2-MIL-125 is indicated by the blue square. Other colors used are as follows: oxygen – red; carbon – cyan; titanium – pink; nitrogen – blue; hydrogen – white. Bottom panel: Pore size distribution from the Poreblazer code.

179x249mm (102 x 102 DPI)

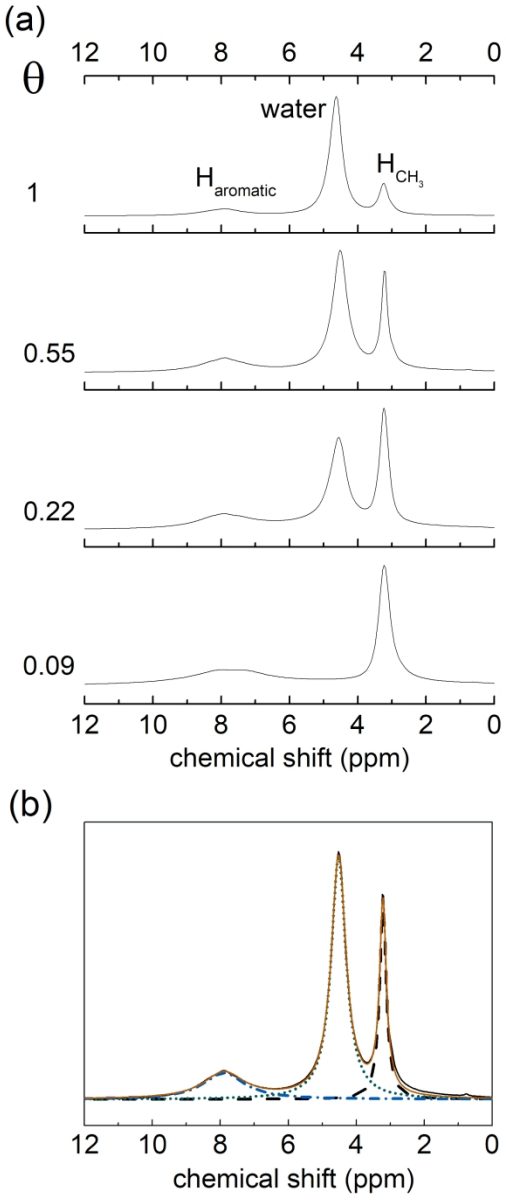

Figure 2. (a) Central band of ^{1}H MAS spectra of NH_2-MIL-125 at different hydration levels expressed through the pore-filling factor θ. The three main signals are assigned to hydrogen atoms of water, of the linker aromatic ring ($H_{aromatic}$), and of methyl groups in residual methanol (H_{CH3}). (b) Spectrum at θ=0.55, showing the Lorentzian peaks obtained from a deconvolution; the green short dotted peak centered at 4.5 ppm is due to water, the blue short dash dotted peak centered at 7.9 ppm is due to $H_{aromatic}$, and the black dashed peak centered at 3.1 ppm is due to H_{CH3}. The sum of the peaks is displayed as a red solid line.

93x186mm (600 x 600 DPI)

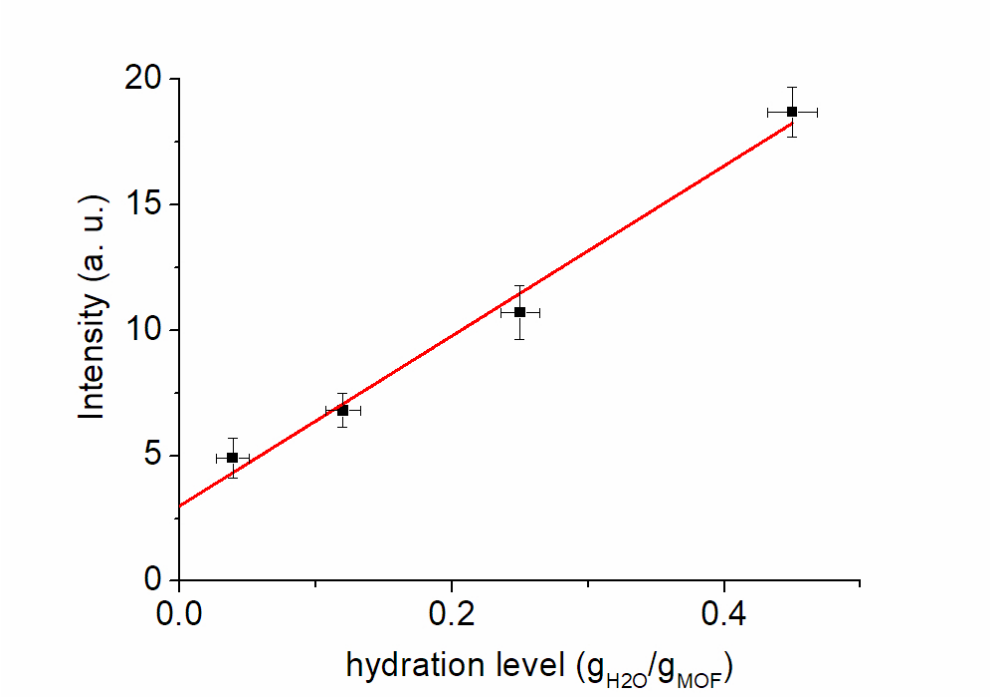

Figure 3. Intensity of the ^{1}H signal resonating at 4.5 ppm as a function of the hydration level expressed in grams of water per grams of dry MOF. The intensity of this peak is scaled imposing that the residual methanol signal intensity is equal to 3, the number of methyl protons for each BDC unit. The line represents the linear fitting curve, characterized by an intercept of 3.0±0.7.

84x59mm (300 x 300 DPI)

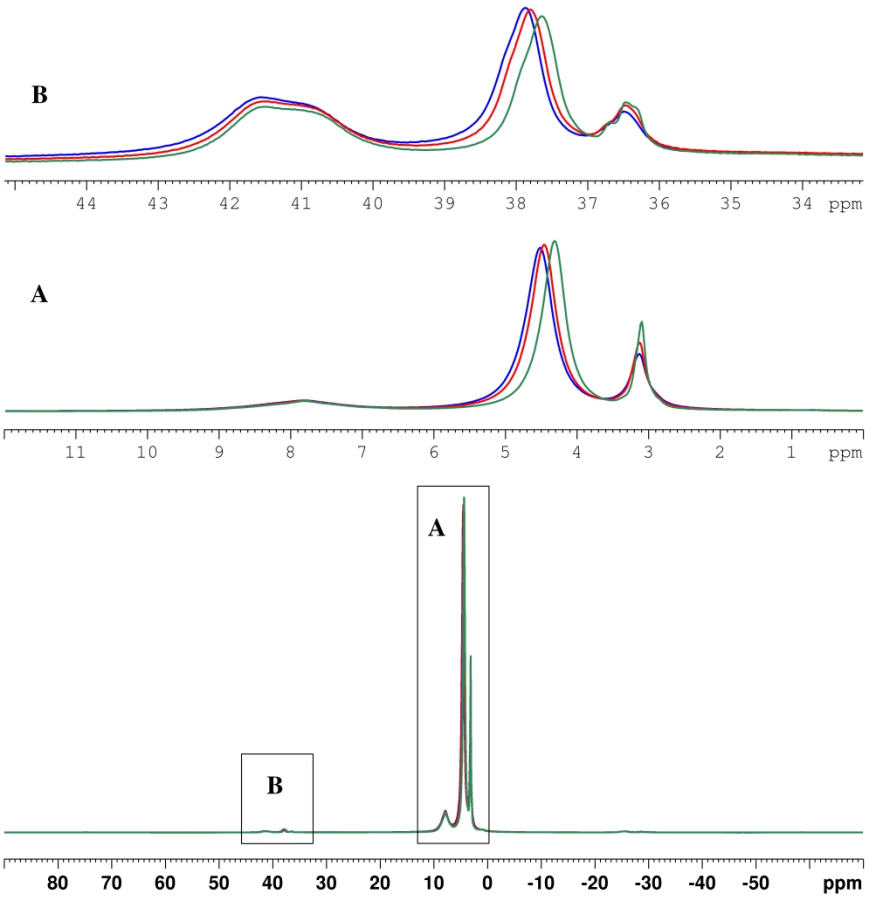

Figure 4. ^{1}H MAS spectra of NH_2-MIL-125 at θ=1 at 25 (blue line), 40 (red line) and 80 (green line) °C (lower trace) and expansion of the central band labeled A (middle trace) and of the first order side band on the left side labeled B (upper trace). The vertical scale in the upper trace is decreased by a factor of 95 compared to that of the lower trace.

184x174mm (720 x 720 DPI)

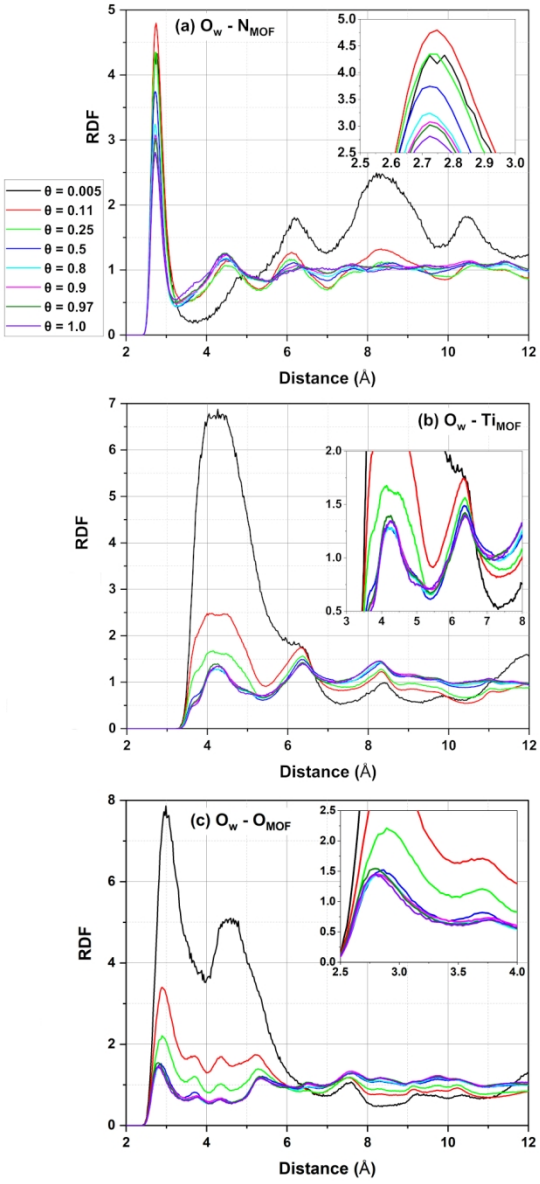

Figure 5. RDFs of three atomic pairs: oxygen of water with nitrogen of MOF (a), oxygen of water with titanium of MOF (b), oxygen of water with oxygen of the hydroxyl groups of MOF (c). The insets show some additional details of the first peaks.

83x172mm (300 x 300 DPI)

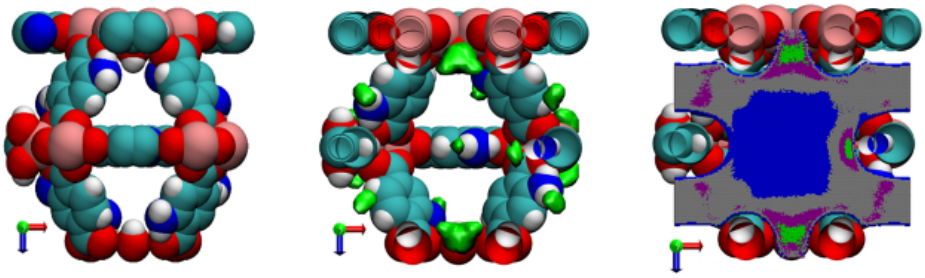

Figure 6. Free energy landscape analysis in NH_2-MIL-125. In the centre: most favourable interactions sites shown as green regions (from -40 to -30 kJ/mol). On the right: an x-z plane slicing through the centre of octamer Ti window. Colours represent the values of free energy: grey and blue from -20 to -10 and from -10 to 0 kJ/mol, respectively; purple from -30 to -20 kJ/mol; green from -40 to -30 kJ/mol. Colors for the atoms of the structure are as in Figure 1.

178x69mm (96 x 96 DPI)

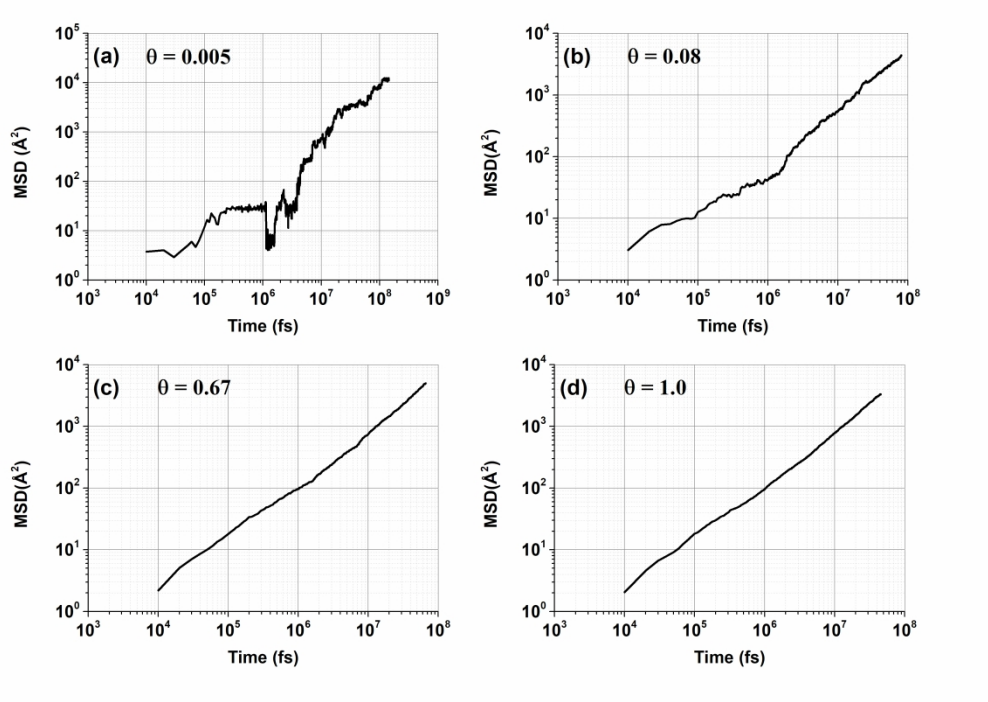

Figure 7. MSD of water in NH_2-MIL-125 as a function of time for selected relative loadings θ at 25 °C.

169x119mm (600 x 600 DPI)

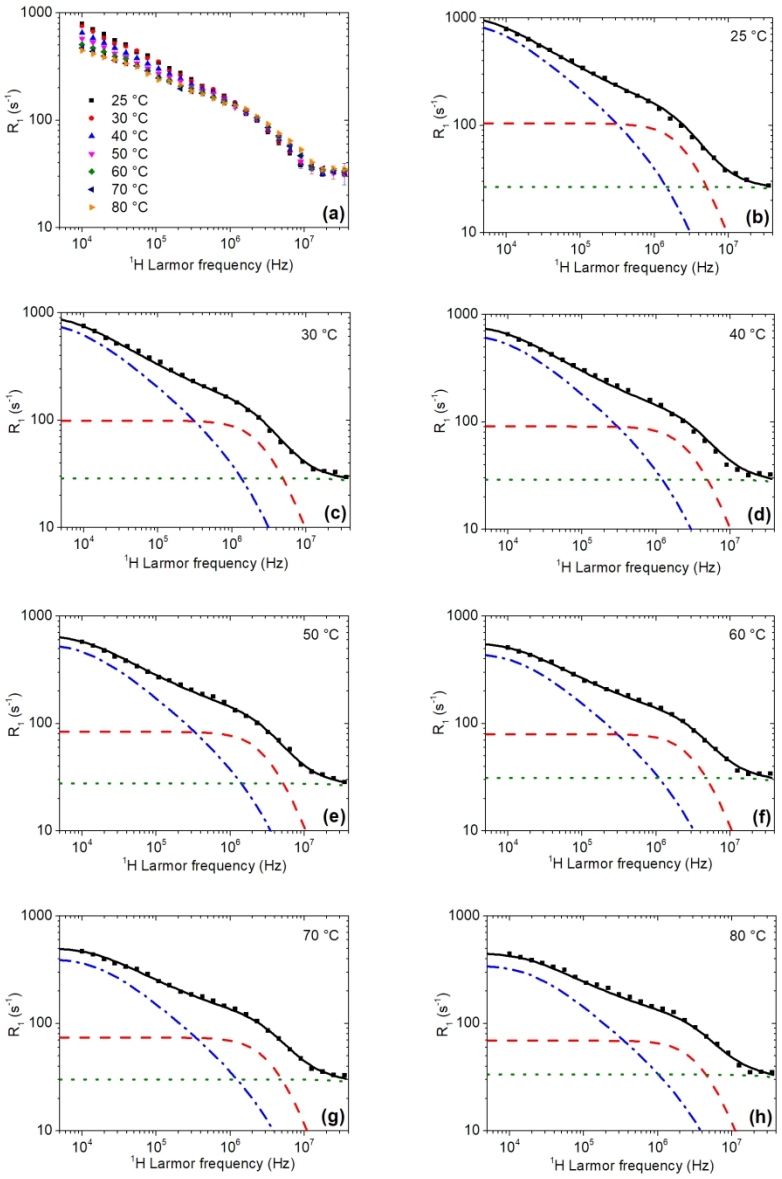

Figure 8. (a) Experimental R_1 NMRD curves of completely hydrated NH_2-MIL-125 at the indicated temperatures. (b)-(h) Comparison of the experimental (squares) and calculated (black line) R_1 NMRD curves at each temperature. Blue dash-dotted, red dashed, and green dotted lines represent contributions to R_1 from RMTD mechanism, anisotropic and isotropic rotational dynamics, respectively.

177x240mm (300 x 300 DPI)

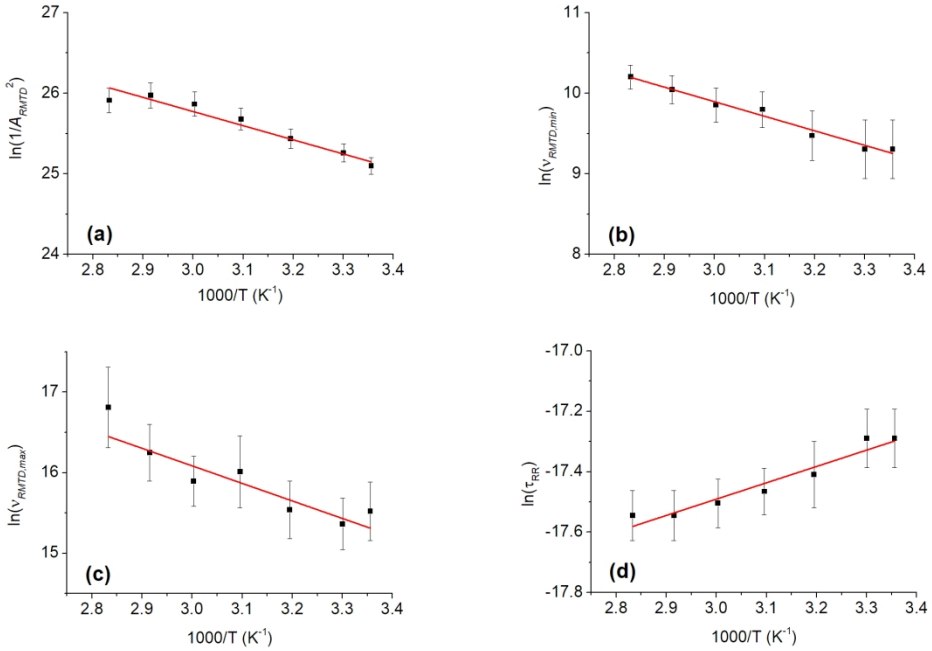

Figure 9. Temperature trend of the fitting parameters $1/A_{RMTD}^2$, $\nu_{RMTD,min}$, $\nu_{RMTD,max}$, and τ_{RR} in panels a, b, c, and d, respectively). The straight red lines represent Arrhenius fits with activation energies of 15 ± 1 kJ/mol, 15 ± 1 kJ/mol, 18 ± 4 kJ/mol, and 4.5 ± 0.5 kJ/mol for panel a, b, c, and d, respectively.

177x119mm (300 x 300 DPI)

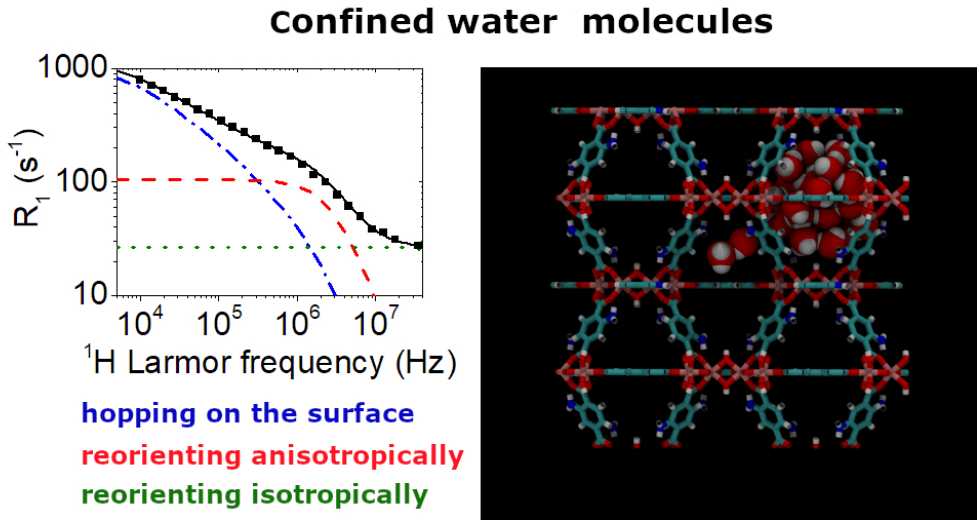

82x44mm (300 x 300 DPI)